



저작자표시-비영리-변경금지 2.0 대한민국

이용자는 아래의 조건을 따르는 경우에 한하여 자유롭게

- 이 저작물을 복제, 배포, 전송, 전시, 공연 및 방송할 수 있습니다.

다음과 같은 조건을 따라야 합니다:



저작자표시. 귀하는 원저작자를 표시하여야 합니다.



비영리. 귀하는 이 저작물을 영리 목적으로 이용할 수 없습니다.



변경금지. 귀하는 이 저작물을 개작, 변형 또는 가공할 수 없습니다.

- 귀하는, 이 저작물의 재이용이나 배포의 경우, 이 저작물에 적용된 이용허락조건을 명확하게 나타내어야 합니다.
- 저작권자로부터 별도의 허가를 받으면 이러한 조건들은 적용되지 않습니다.

저작권법에 따른 이용자의 권리는 위의 내용에 의하여 영향을 받지 않습니다.

이것은 [이용허락규약\(Legal Code\)](#)을 이해하기 쉽게 요약한 것입니다.

[Disclaimer](#)

Ph. D. DISSERTATION

**ENHANCED PERFORMANCE OF
INKJET PRINTED QUANTUM DOT
LIGHT EMITTING DIODES**

잉크젯 양자점 발광 다이오드의 성능 향상에
대한 연구

BY

HEEBUM ROH

FEBRUARY 2021

DEPARTMENT OF
ELECTRICAL AND COMPUTER ENGINEERING
COLLEGE OF ENGINEERING
SEOUL NATIONAL UNIVERSITY

ENHANCED PERFORMANCE OF INKJET PRINTED QUANTUM DOT LIGHT EMITTING DIODES

잉크젯 양자점 발광 다이오드의 성능 향상에
대한 연구

지도교수 곽 정 훈

이 논문을 공학박사 학위논문으로 제출함

2021년 2월

서울대학교 대학원

전기정보 공학부

노희범

노희범의 공학박사 학위논문을 인준함

2021년 2월

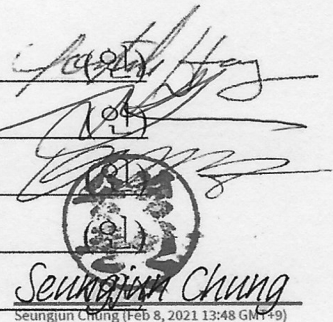
위원장 : _____ 홍 용 택

부위원장 : _____ 곽 정 훈

위원 : _____ 이 재 상

위원 : _____ 송 형 준

위원 : _____ 정 승 준



Seungjun Chung
Seungjun Chung (Feb 8, 2021 13:48 GMT+9)

Abstract

EHNACED PERFORMANCE OF INKJET PRINTED QUANTUM DOT LIGHT EMITTING DIODES

HEEBUM ROH

DEPARTMENT OF ELECTRICAL AND

COMPUTER ENGINEERING

COLLEGE OF ENGINEERING

SEOUL NATIONAL UNIVERSITY

Colloidal quantum dot light-emitting diodes (QLED) are promising next-generation displays, exhibiting excellence in color purity, low material cost possibility, brightness. Quantum dots, which have many advantages, require patterning technology because of their colloidal status. Various patterning method for colloidal QD have been proposed using drop-casting, mist coating, transfer printing, inkjet printing. Drop casting method can fabricate fast but having weakness in large area process. Mist coating method might be made a

monolayer deposition with high accuracy but difficulty in high resolution. Transfer printing method is possible to highest resolution patterning in technologies but having an ink contamination issue. However, ink-jet printing technology is emerging interest for the fabrication of QLEDs because of advantages such as high-resolution pattern possibility, fast processability and tiny material usage by drop-on-demand process.

To fabricate high performance QLEDs using inkjet-printing technology, there are some challenges. First is morphology issue which goal is achieving a uniform film deposition against coffee ring effect and bad roughness. Second is a printing failure, which considering accurate positioning of the ink droplet against the angular deviation of the droplet leaving nozzle of the inkjet cartridge. This droplet deflection may be caused by nozzle clogging, machine tremor and error occurrence in inkjet-printing machine, and it leads to two problem such as mis-aiming and overflow. Third is a jeattability for forming a stable drop at nozzle. This is determined by rheological parameters such as viscosity, inertial force, and surface tension. Final is solvent limits which are not dissolving the underlayer, preventing QD aggregation and toxicity to human. There have been studies related to enhancement of inkjet printed QLED by using solvent mixture to form uniform film or using hydrophobic walls to prevent from mis-aiming and overflow, but the reported performance of inkjet-printed QLED is still low. For the practical use of inkjet-printed QLEDs, it is prerequisite to resolve the morphology issue against coffee-ring

effect and the printing failure in the relation with the performance of inkjet printed device.

In this study, we improved the EQE and CE of inkjet-printed QLED device using hydrophobic walls and QD-polymer composite ink. Hydrophobic walls are used making the droplet positing precise within the bank and it is evaluated a photolithographic property and the resistivity on the printing failure of this material. QD-polymer composite ink can increase viscosity of ink and induce the additional polymer Marangoni effect. When using hydrophobic walls, printed QD ink with the angular deviation is positioned well in the bank and prevent from the overflow out of emission area. Well defined ink induces the pixel uniformity of devices and resulted QLED exhibit the maximum luminance of 5300 cd m^{-2} and the external quantum efficiency of 0.11 %. Despite of these relatively low performance, it shows the resistivity of printing failure, so I believe it can be further improved through elaborated optimization.

Also, when PMMA is added in the QD ink, the QD-polymer composite ink can reduce the coffee-ring effect and form a uniform thin film. Pile-up at the bank wall is also reduced by additional polymer Marangoni effect. In addition, PMMA of suitable polymer chain length can reduce the surface roughness, thereby improving the morphological properties of the thin film. The resulting inkjet-printed QLED emit the highest luminance of 73360 cd m^{-2} and the external quantum efficiency of 2.8 %, which are conspicuously higher than that of the inkjet-printed QLED without polymer additives.

These results in this thesis show the impact of printing accuracy and uniform film formation, and suggest these methods will promise the high performance of inkjet printed QLEDs.

Keywords: Colloidal Quantum Dot, Light-Emitting Diodes, Inkjet Printing, Hydrophobic polymer, Bank engineering, QD-polymer composites, Coffee ring effect

Student Number: 2014-22556

Contents

Abstract	i
Contents	vi
List of Figures	x
List of Tables	xv
Chapter 1	1
1.1 Colloidal Quantum Dots.....	1
1.2 Fabrication Technology of QLEDs	6
1.3 Key Issues for Inkjet-printed QLED Performance ..	8
1.4 Outline of Thesis.....	11

Chapter 2. Experimental Methods	14
2.1 Materials	14
2.1.1 Red-color Emitting CdSe/Zn_{1-x}Cd_xS Core/shell Heterostructured Quantum Dots	14
2.1.2 Fluorinated photopolymer, PFBI.....	16
2.1.4 Organic Material.....	16
2.1.3 Preparation of ZnO Nanoparticels.....	17
2.2 Device Fabrication and Characterization Methods..	18
2.2.1 Device Fabrication.....	18
2.2.2 Current-voltage-luminance Measurement.....	18
2.2.3 Efficiency Calculation Methods	22
2.2.3 Other Characterization Methods.....	22
2.3 Theory	24
2.2.1 Surface Energy Analysis.....	24
2.2.2 Coffee Ring Effect and Capillary Flow	25
2.2.3 Marangoni Flow.....	26

Chapter 3. Printing Accuracy Improvement of Inkjet-printed QLED with Engineered Bank using PFBI as Highly Fluorinated Photopolymer **27**

3.1 Introduction.....30

3.2 Evaluation of Pixelated Structure with PFBI.....31

3.3.1 Highly Fluorinated Photopolymer, PFBI for Inkjet-printed QLEDs 32

3.3.2 Characteristics of Pixelated Structure made of PFBI... 33

3.3 Evaluation of QD Inks on Pixelated Structure with PFBI..38

3.3.1 Morphology Properties of QD Inks on Pixelated PFBI Structure 40

3.3.2 Characteristics of Inkjet-printed QLED using PFBI.... 43

3.3 Summary.....47

Chapter 4. Efficiency Improvement of Inkjet-printed QLEDs Employing Polymer Additives **48**

4.1 Introduction of Inkjet-printed QLEDs50

4.2 Evaluation of QD-PMMA Composite Ink on Planar Substrate	54
4.2.1 QD-PMMA Composite Ink for Reducing Coffee Ring Effect	54
4.2.2 Morphology Uniformity of QD Droplet Film using PMMA Additives	59
4.3 Evaluation of QD-PMMA Composite Ink on Pixelated Structure	64
4.3.1 Morphology Properties of QD Inks on Pixelated Structure	64
4.3.2 Electrical Characteristics of Inkjet-printed QLEDs Employing PMMA Additives	68
4.6 Summary	77
Chapter 5	78
Bibilography	81
Publication	85
한글 초록	88

List of Figures

Figure 1.1 (a) Comparison of red, green and blue EL spectra with (dashed lines) OLEDs and (solid lines) QD-LEDs [4]. (c) The CIE (Commission Internationale de l’Eclairage) 1931 chromaticity diagram. As full-width-half-maximum of the quantum dot narrows from 60 to 25 nm, the simulated spectral locus grows close to the edge of the CIE diagram. Simulations assume a Gaussian QD emission profile. [14].	3
Figure 1.2 QLED and OLED (a) application on the premium TVs and (b) composition.	4
Figure 1.3 Patterning technology of colloidal QDs (a) Drop casting (b) Mist coating (c) Transfer printing (d) Inkjet Printing	7
Figure 2.1 (a) Photo-responsivity curve of PFBI. (b) Scanning electron microscope (SEM) image of patterned PFBI film on Si wafer. (c) Cross-sectional view of (i) section, 7 μm half-pitch pattern (d) Magnification of (ii) section, 7 μm half-pitch pattern	15
Figure 2.2 Chemical structures of CBP and PMMA	16
Figure 2.3 The CIE standard observer color matching functions	20
Figure 2.4 Description of surface tension	24
Figure 3.1 (left – right) Schematic of mechanism of mis-aiming, which means droplet landing in an incorrect position	28

Figure 3.2 (left – right) Concept art of compensation for printing failure such as mis-aiming and overflow	31
Figure 3.3 Photography of (a) deionized water and (b) diiodomethane droplets on top of PFBI for measuring the contact angles between droplet and thin films; Calculated surface energy is 17.5 mJ/m ² by Owens and Wendt model.	31
Figure 3.4 Well formation of bank structure. (a) Optical microscope image, (b) SEM image of cross-sectional bank. (c) AFM morphology image of active area after development of PFBI with 1.84 nm of rms value, (d) Profile image of cross-sectional bank indicating 1.5 μm of height.....	34
Figure 3.5 The droplet image of printed QD ink on PFBI substrate (right gray region) and ITO (left bright region). Red line is an actual printing position. Blue line is a desired printing position. Green arrow means compensation of Mis-aiming by hydrophobic property of PFBI.....	36
Figure 3.6 The droplet image of printed QD ink on (a) conventional PI bank and (b) PFBI bank. The hydrophobic property of PFBI prevents from the overflow of printed QD ink in same volume.....	36
Figure 3.7 The droplet image of printed QD ink (dual solvent; CHB:DCB = 8:2) on PFBI bank; (left) optical microscope image; (right) Photoluminescence image.....	39
Figure 3.8 Scheme of how to be made the dome shape film formation.....	39
Figure 3.9 Scheme of how to alleviate the dome shape film formation.....	40
Figure 3.10 The droplet image of printed QD ink (single solvent; isoparaffine case) on PFBI bank; (left) optical microscope image; (right) Photoluminescence image.....	42

Figure 3.11 The droplet image of printed QD ink (single solvent; isoparaffin case) on PFBI-1 bank patterned by elliptical for ink wetting; (a) just printed; (b) dried; (c) optical microscope image; (d) profiler image;.....	43
Figure 3.12 Fabrication process of inkjet printed QLED device using PFBI-1 bank. (1) Development in fluoruous solvent. (2) Solvent drying. (3) Vacuum deposition of CBP, MoO ₃ and Al	44
Figure 3.13 Schematic illustration of inverted structure of QLEDs and inkjet-printing on pixelated PFBI structure	45
Figure 3.14 Electrical characteristics of inkjet printed QLEDs with PFBI-1 bank; (a) current density-voltage (J-V) characteristics: (b) luminance-voltage (L-V) characteristics: (c) EQEs versus the current density curve; (d) Electroluminescence spectrum.	46
Figure 4.1 Schematics of the reason why inkjet printed QD films using dual solvent still have rough morphology in the case of pixelated device, leading to inferior performance of full device.....	53
Figure 4.2 Schematics of the reason why inkjet printed QD films using dual solvent have better morphology in the case of non-pixelated device, leading to relatively good performance of full device; the solvent of high boiling point is expelled from center to edge of films.	53
Figure 4.3 (a) Absorbance, (b) PL spectrum, and (c) Transient PL of pristine QD ink and QD + PMMA inks (Mw: 2 kDa, 8 kDa, and 350 kDa, respectively).	56
Figure 4.4 Measurement of contact angle of QD ink without and with PMMA varying the molecular weight of PMMA on (upper) silicon substrate and (lower) SAM treated substrate; (left to right) pristine QD ink and QD + PMMA inks (Mw: 2 kDa, 8 kDa, and 350 kDa, respectively).	57

Figure 4.5 Weber number vs. Reynolds numbers of the pristine QD inks and the QD–PMMA (Mw of 2, 8, and 350 kDa) composite inks, indicating that all the inks are in the printable zone.....	58
Figure 4.6 Electrical performance comparison of QD solution dissolved in (black) toluene and (red) CHB : DCB = 8 : 2 mixture in case of spin-coated QLEDs.....	59
Figure 4.7 Photoluminescent image of printed QD droplets on ZnO NPs film induced by the 360 nm laser with (a) Pristine QD ink and (b) QD - PMMA composite inks (Mw: 8 kDa).	60
Figure 4.8 The height profile and the 3D morphology images of each droplet from the QD inks (a) without and (b) with PMMA (Mw = 8 kDa)	62
Figure 4.9 Timeline images of drying process for emissive dots using (top) pristine QD ink, (bottom) QD + PMMA ink (Mw : 8 kDa); The time moves from left to right on the timeline.	63
Figure 4.10 (a) Microscope image of subpixel (left) and with inkjet-printed QD films on the bank covered with ZnO NPs (right); yellow line indicates dimensions of sub-pixel; red line indicates outline for optical profile of horizontal axis, (b) Optical profiles of inkjet-printed films using pristine QD ink and QD + PMMA inks (Mw: 2 kDa, 8 kDa, and 350 kDa, respectively).	66
Figure 4.11 AFM images of films using (a) pristine QD ink and QD + PMMA inks (Mw: 2 kDa, 8 kDa, and 350 kDa, respectively), which are inkjet-printed on the bank structure covered with ZnO NPs.....	67
Figure 4.12 (a) Current density–voltage characteristics (inset for a low voltage region), (b) luminance–voltage characteristics, (c) EQE– current density, and (d)	

the EL spectra of the inkjet-printed QLEDs using the pristine QD ink and the QD-PMMA inks.....	72
Figure 4.13 Electroluminescence image of (a) pristine QD and (b) QD + PMMA (8 kDa of molecular weight).....	73
Figure 4.14 Lifetime comparison of pristine QD and QD + PMMA (2 kDa, 8 kDa and 350 kDa of molecular weight). Device lifetime equals device performance trend.....	74
Figure 4.15 (a) Current density-voltage characteristics (inset for a low voltage region), (b) luminance-voltage characteristics, and (c) EQE-current density of the spin-coated QLED and inkjet-printed QLEDs using toluene, mixture and mixture containing polymer additive (Mw: 8 kDa), respectively..	75

List of Tables

Figure 1.1 (a) Comparison of red, green and blue EL spectra with (dashed lines) OLEDs and (solid lines) QD-LEDs [4]. (c) The CIE (Commission Internationale de l’Eclairage) 1931 chromaticity diagram. As full-width-half-maximum of the quantum dot narrows from 60 to 25 nm, the simulated spectral locus grows close to the edge of the CIE diagram. Simulations assume a Gaussian QD emission profile. [14].
.....4

Figure 1.1 (a) Comparison of red, green and blue EL spectra with (dashed lines) OLEDs and (solid lines) QD-LEDs [4]. (c) The CIE (Commission Internationale de l’Eclairage) 1931 chromaticity diagram. As full-width-half-maximum of the quantum dot narrows from 60 to 25 nm, the simulated spectral locus grows close to the edge of the CIE diagram. Simulations assume a Gaussian QD emission profile. [14].....4

Figure 1.1 (a) Comparison of red, green and blue EL spectra with (dashed lines) OLEDs and (solid lines) QD-LEDs [4]. (c) The CIE (Commission Internationale de l’Eclairage) 1931 chromaticity diagram. As full-width-half-maximum of the quantum dot narrows from 60 to 25 nm, the simulated spectral locus grows close to the edge of the CIE diagram. Simulations assume a Gaussian QD emission profile. [14].....4

Figure 1.1 (a) Comparison of red, green and blue EL spectra with (dashed lines) OLEDs and (solid lines) QD-LEDs [4]. (c) The CIE (Commission Internationale de l’Eclairage) 1931 chromaticity diagram. As full-width-half-maximum of the quantum dot narrows from 60 to 25 nm, the simulated spectral locus grows close to the edge of the CIE diagram. Simulations assume a Gaussian QD emission profile. [14].....4

Chapter 1

Introduction

1.1 Colloidal Quantum Dots

Colloidal quantum dot (QD) has largely attracted for promising future display technology since it reported in 1980's by Alexey Ekimov [1] and Louis Brus [2]. QDs have several unique properties like wide absorption, narrow emission spectra, tunable emission wavelength by core size and composition control, and solution capability [3-6]. By these characteristics, QDs have made efforts to adopt widespread fields such as light-emitting diodes (LEDs) [7-10], bioimaging [11], solar cells [12], sensing applications [13], e

t

cetera. Especially, QDs based light-emitting-diodes (QLEDs) are believed to outperform their competitors in display area by taking the advantages of high

color purity and quantum efficiency. And QLED has the same structure as currently commercialized organic light-emitting diodes (OLEDs), so there is little need to change the production line. Additionally, the inherent solubility of colloidal QD by surface ligands is enabled to large-area, flexible displays with low material loss using solution-based printing methods [ref].

Currently, OLED has begun to be used in the display market in earnest. However, the broad emission width of the organic luminary is an insurmountable weakness though recent advance in the OLED technology. The usual full width at half maximum (FWHM) of OLED is greater than 40 nm due to the vibronic state of organic dyes, but, that of QLED is less than 30 nm. Figure 1.1b shows the narrow EL spectra of QD-LEDs compared to that of typical OLEDs. Figure 1.1 c exhibit the narrow bandwidth feature of QD emitter leads to widening of the color reproducible range in the color gamut. These virtues in QDs make QD-LEDs as high color purity and excellence in color gamut, which is better than most of commercialized displays, and as convincing candidate for next-generation display and light source.

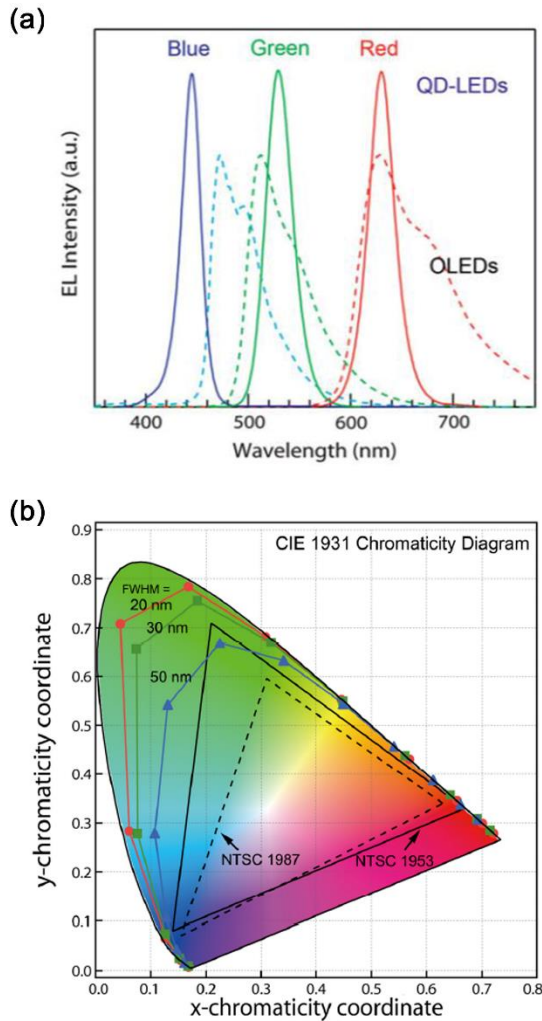


Figure 1.1 (a) Comparison of red, green and blue EL spectra with (dashed lines) OLEDs and (solid lines) QD-LEDs [4]. (c) The CIE (Commission Internationale de l'Eclairage) 1931 chromaticity diagram. As full-width-half-maximum of the quantum dot narrows from 60 to 25 nm, the simulated spectral locus grows close to the edge of the CIE diagram. Simulations assume a Gaussian QD emission profile. [14].

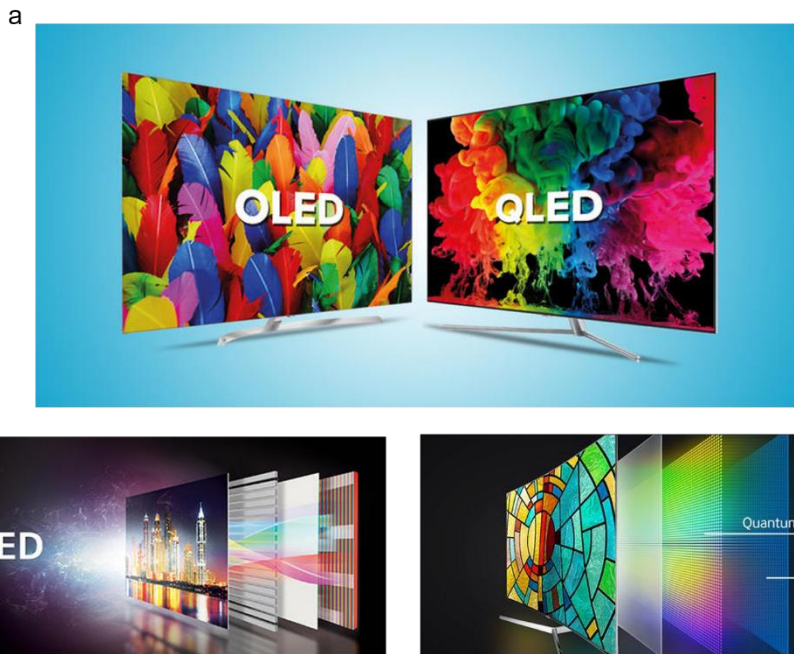


Figure 1.2 QLED and OLED (a) application on the premium TVs and (b) composition
(Pictures are referred to following websites: www.insidevina.com, www.stuff.tv)

Currently, the main providers of QD technology for use in TVs are Nanosys and 3M, which provide the Quantum Dot film (QDEF) option for use with Full Array backlit LED/LCD TVs. The use of QDs has taken a big leap forward as several TV makers have shown off Quantum Dot-enabled TVs at tradeshows including Samsung, TCL, Hisense/Sharp, Vizio, and Philips. Samsung and Vizio have brought models to market in the U.S. QLED TVs are much more similar to traditional LED TVs: they have an LED backlight behind a layer of pixels that generates the picture. However, unlike traditional LED TVs, they use quantum dots as a filter to produce more accurate and better saturated colors. Furthermore, while their response time is very good, they don't suffer from the same stuttering that OLED TVs do. Their black levels are good for an LED TV and viewing angles are more akin to LED TVs as well.

While OLED is able to make screens much darker for better contrast, QLED display screens are a lot brighter. This makes it ideal for brighter rooms and content that are HDR. They also come in various sizes, big to small, and is also a lot more affordable in comparison to OLEDs. To compare, Samsung's QLED TVs come in 43-inch to 98-inch sizes. This is an advantage as large televisions are the fastest-growing segment of the market, which makes Samsung the better option in this aspect. It also has the better outlook in being able to evolve further and better, as Samsung has revealed a version of QLED that does use emissive technology, much like OLED and plasma. Known as direct-view

quantum dot, it dispenses with the liquid crystal layers and uses quantum dots themselves as the light source.

1.2 Fabrication technology of QLEDs

Unlike OLED fabrication, Colloidal QDs can only be implemented in a solution process due to their inherent soluble property by surface-stabilized ligands. So, patterning of QD is important in the realization of QLED for the next generation display. Thus, various patterning methods have been proposed using drop casting, mist coating, transfer printing and inkjet printing. Drop casting method containing spin coating is the most powerful approach in the laboratories due to the simple, fast and precise thickness controllable process. However, it is not suitable for large area display and mass manufacturing line. Mist coating, also known as spray coating, was originally used for by spraying the liquid type chemical with inert gas to form ultra-thin layer. It is capable of high-precision monolayer deposition, but is difficult to apply to high resolution displays. Transfer printing is using soft and elastomeric stamps to move the pre-patterned materials. This technology can employ high resolution patterning but needs to overcome critical problems such as particle contaminations and sagging of elastomeric stamps. Inkjet printing is a non-contact and mask-free approach for the formation of thin film with the pixelated structure [ref]. The Inkjet printing process dispenses ink droplets from nozzle which is controlled by electrical signals. Dispensed ink droplets are

precisely control falling to specified positions of a substrate, then spreading and drying to form thin films. Especially, inkjet printing using piezoelectric technique employ drop-on-demand control which minimizing material loss. The remarkable characteristics of inkjet technology with these advantages are attracting attention to the fabrication process of QD for future display.

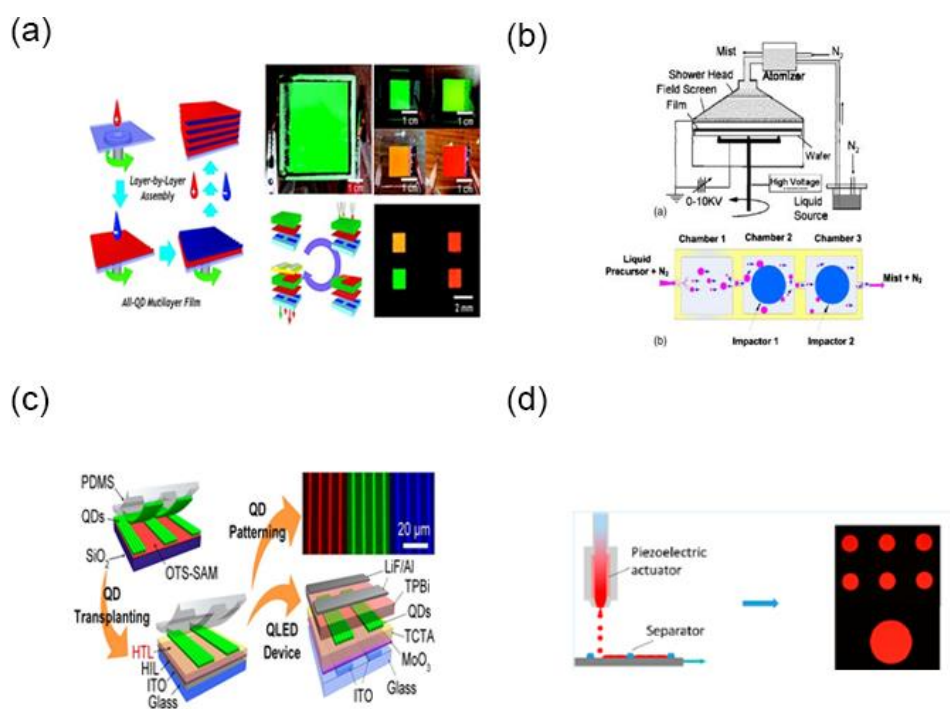


Figure 1.3 Patterning technology of colloidal QDs (a) Drop casting (The image is taken from ref. [15]) (b) Mist coating (The image is taken from ref. [16]) (c) Transfer printing (The image is taken from ref. [17]) (d) Inkjet printing (The image is taken from ref. [18])

1.3 Key issues for Inkjet-printed QLED performance

The excellent solution processability of colloidal QDs facilitates direct patterning of RGB pixels via inkjet printing. Two critical issues need to be taken into consideration to obtain uniform QD films with controllable thickness. The first issues are to avoid re-dissolution of layers during device processing. The OLED field has achieved considerable successes in the deposition of multi-layers from solutions. Nevertheless, inkjet-printing processes require ink with controlled solution properties, such as concentration, surface tension and viscosity, which bring extra difficulties in formulation of QD inks. The second challenge is to minimize coffee ring effect, i.e. concentrate particles at the rim of a dried liquid droplet. In 2009, Jabbour and co-workers demonstrated fabrication of QLEDs having pixelated arrays of QDs films deposited by inkjet printing [19]. Chlorobenzene, a low-vapor-pressure solvent, was used to deposit QD films, aiming to reduce coffee-ring effects. However, chlorobenzene interacted with the underneath p-TPD layer, causing QD films with poor morphologies, such as high surface roughness and existence of voids. As a result, QLEDs exhibited relatively high driving voltages and exciplex emission due to direct contact of p-TPD (HTL) and TPBI (ETL) layers. In recent work, Jiang et al. fabricated inverted QLEDs by inkjet printing with a mixed solvent of 1,2-dichlorobenzene in cyclohexylbenzene with an optimal ratio of 20 vol% to reduce surface tension. Encouragingly, coffee-ring-free QD films were obtained. The respective device exhibited a peak efficiency of 4.5 cd A^{-1} and maximum brightness of $12,000 \text{ cd m}^{-2}$.

Rogers and co-workers employed electrohydrodynamic jet printing, i.e. e-jet printing, to deposit homogenous arrays of QD patterns over thickness. This work demonstrated high-levels of resolution achievable for printing techniques.

Inkjet printing of QDs is highly advantageous for implementing full-color displays, attributed to the fast process time and the minimal material usage by drop-on-demand process with high precision and accuracy [22,23]. In addition, since this method does not require an individual fine metal mask for RGB colors, it is advantageous for the production of large-area displays. On the other hand, inkjet printing poses a widely known issue, which is non-uniformity, caused by the coffee-ring effect [36–39]. Uniformity of inkjet-printed surface morphology has been thoroughly studied, with many available reports examining its improvement. Towards this direction, a widely used method is by controlling the Marangoni effect [40–42] of the droplet, via using co-solvents [24–35], mixing surfactants[43–46], and/or fine-tuning viscosity [47–50]. For instance, Jiang et al. reported the construction of inkjet-printed QLEDs with the EQE of 1.1% and maximum luminance (L) of 12000 cd m⁻², using a binary co-solvent consisting of cyclohexylbenzene (CHB) and 1,2-dichlorobenzene (o-DCB) [24].

1.4 Outline of Thesis

This thesis consists of five chapters, including the Introduction and Conclusion. As an introduction, Chapter 1 describes the previous research on colloidal quantum dots, patterning technology of quantum dot, fabrication technology of QLEDs and the key issues for inkjet printed QLEDs performance. Chapter 2 includes the methods for preparing materials: the methods used to the highly luminescent type-I red hetero-structured QDs; the organic materials; the fluorinated resist; and the preparation of ZnO nanoparticles used in this thesis are described in detail. In addition, the fabrication and characterization methods for the inkjet printed QLED devices are summarized in this chapter, and the electrical and morphological characterization methods for thin films used in this thesis are depicted. Characterization methods for electrical and morphological characteristics of thin films are also described in this Chapter. In Chapter 3, the influence of fluorinated photopolymer bank on the electrical performance of the inkjet printed QLED is evaluated. The fluorinated photopolymer, PFBI with low surface energy was developed to compensate for printing failure such as mis-aiming and overflow. The morphological characteristics of pixelated PFBI photopolymer is evaluated to realize the bank structure for inkjet printed QLED. We confirmed the compensation for printing failure on the PFBI bank by artificially mis-aimed droplet of QD ink. In addition, the morphological characteristics of printed QD films on the pixelated PFBI is evaluated by changing the solution of QD ink. We choose the isopraffin as the solution of

QD ink and analyzed the morphological property of QD film with the solution by optical profilometry. And we found the enhanced electrical property of inkjet printed QLED device by forming a uniform film. Enhanced device performance on turn-on voltage, leakage current, efficiency, and luminance were originated from improve the morphology of QD film. In chapter 4, we identify the effect of QD-polymer composite ink on the electrical performance, which could lead to important research in terms on the ink design to further improve inkjet printed QLEDs. There are only a few studies on inkjet-printed QLED with pixelated bank because it is much harder to guarantee the uniformity of an inkjet printed QD films by the inherent drying behavior of QD ink. To resolve the uniformity problem, we added a small amount of polymer into QD ink due to the enhancement of the morphology by filling the gap between QD chunks and the possibility of leading to polymer Marangoni flow. We choose the PMMA due to its high optical transparency and good solubility with used solvent. To identify the effect of QD-polymer composite ink, the morphology of QD droplet and QD film on the pixelated structure is evaluated in relation to the effect on molecular weight variation of PMMA. In addition, the electrical and morphological performance of inkjet printed QLED using QD-polymer composite ink is also analyzed. We found the We isolated electroluminescence and photoluminescence of QDs and QD-LEDs and compared degradation factors in the devices. Finally, in Chapter 5, we summarize our work and present concluding remarks.

Chapter 2

Experimental Methods

2.1 Materials

2.1.1 Red-color Emitting CdSe/Zn_{1-x}Cd_xS Core/shell Heterostructured Quantum Dots

QD synthesis was conducted modifying the method by Kwak et al. and Bae et al. [20,21]. In the comparison of their fluorescence intensities, photoluminescence quantum yield (PL QY) was acquired with those of primary standard dye solution (coumarin 545, quantum yield = 82 % in toluene) at the same optical density (below 0.1) at same excitation wavelength (450 nm). Peak PL intensity and full width half maximum (FWHM) of synthesized QD

was 630 nm and 30 nm, respectively. PL dynamics were measured using time-correlated single-photon counting (TCSPC) system that consists of avalanche photodiodes (timing resolution ~ 350 ps) and a multi-channel analyzer (Picoquant Hydraharp). The measured PL decay time constant (τ_{PL}) is 20.1 ns.

2.1.2 Fluorinated photopolymer, PFBI

A fluorinated photopolymer, P(FOMA-BMOMA-IBMA), called as PFBI, is made by copolymerization of perfluorooctyl methacrylate (FOMA) with benzil mono-oxime methacrylate (BMOMA) and isobornyl methacrylate (IBMA). The molar weight of PFBI is 12,600 by 1H -NMR measurement. The thermal degradation temperature of PFBI was 245 °C and the 10 wt% weight loss occurred about 186 °C from TGA results. The glass transition temperature of PFBI was about 67 °C from the DSC results. Figure 2.1a shows the photoresponsivity characteristics of PFBI polymer and the dose-to-clear of PFBI is about 2.3 J cm⁻². In order to evaluate pattern formation, I used 20 wt/vol% PFBI solution for 1.7 μ m thickness. After spin coating and soft bake at 80 °C for 3 min, UV exposure of 2.3 J cm⁻² and development by dipping in HFE-7300 for 8 min. The resulted pattern was shown in Figure 2.1b to d. Detailed synthesis recipe and characteristics results are acquired from published paper [22].

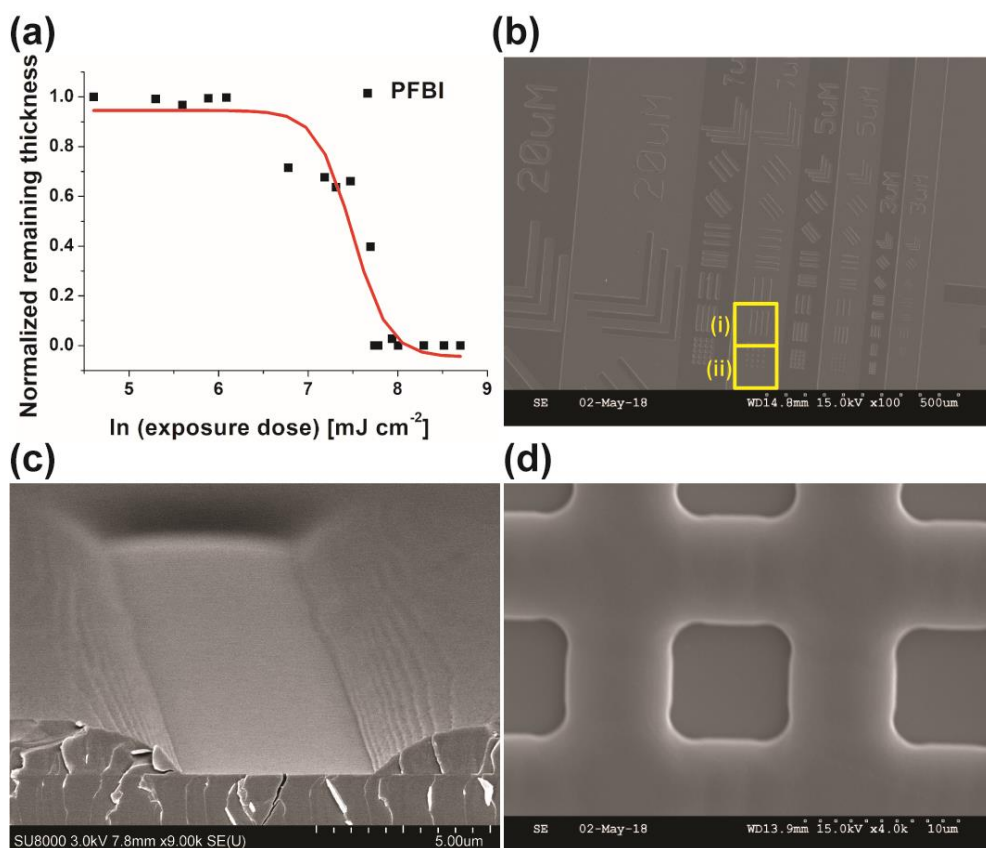


Figure 2.1 (a) Photo-responsivity curve of PFBI. (b) Scanning electron microscope (SEM) image of patterned PFBI film on Si wafer. (c) Cross-sectional view of (i) section, 7 μm half-pitch pattern (d) Magnification of (ii) section, 7 μm half-pitch pattern; Images from published paper [22]

2.1.3 Organic Materials

4,4'-bis(carbazol-9-yl)biphenyl (CBP) are purchased from OSM as hole injection interlayer. Polymer additives (PMMA of different molecular weights)

were purchased from Sigma-Aldrich. Chemical structures of organic materials used in this thesis are as follows.

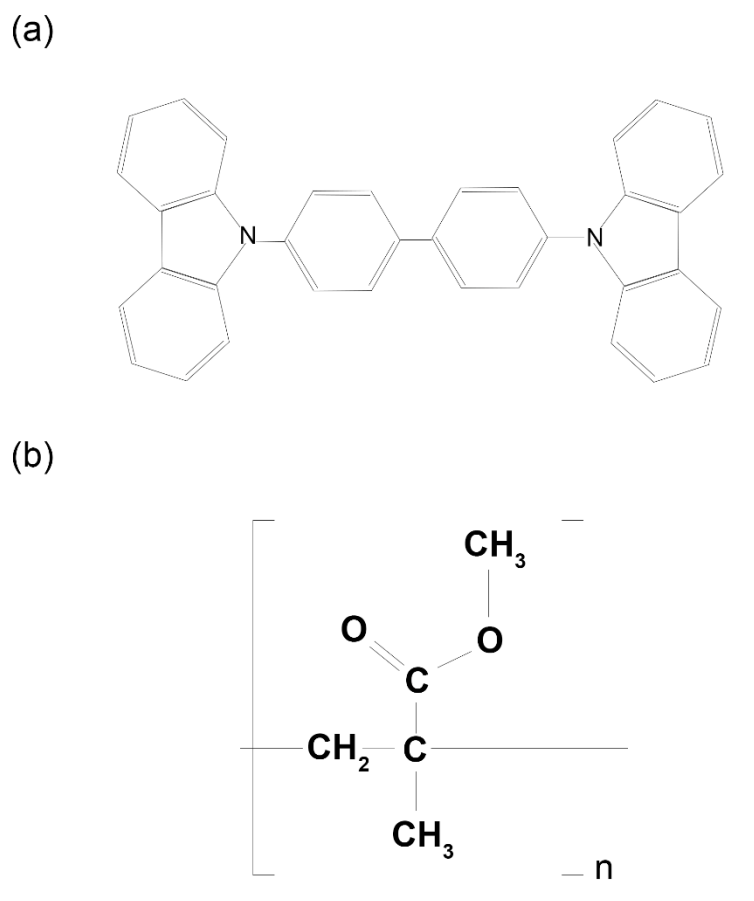


Figure 2.2 Chemical structures of CBP and PMMA

2.1.4 Preparation of ZnO Nanoparticles

ZnO nanoparticles were synthesized in the modified method reported by Pacholski *et al.*[23] 2 g of Zn(Ac)₂·2H₂O was dissolved in 80 ml of methanol in a 3-neck flask. 65 ml of a methanol solution containing 1.51 g of KOH was added dropwise at 60 °C under strong agitation. And then, this mixture was kept at 60 °C for 2 h 30 min to yield milky solution under N₂ atmosphere. The ZnO nanoparticles appeared as white precipitate in this milky solution and were collected by centrifugation at 4000 rpm after repetitive methanol washing. Finally, 0.1 ml of butylamine was added for stabilization and the precipitate was redispersed in butanol (20 mg ml⁻¹).

2.2 Device Fabrication and Characterization

Methods

2.2.1 Device Fabrication

All QD-LED devices were basically fabricated using the inverted structures and the detail structures, materials and processes are introduced in each chapter. First of all, patterned ITO glass substrates were prepared, which were cleaned with acetone, isopropanol and deionized water in an ultrasonicator (Branson 5510). And then the cleaned ITO glass substrates were dried in the oven at 120 °C. For the inverted structure, 20 mg mL⁻¹ of the ZnO nanoparticle solution was spin-coated on a patterned ITO glass with a spin-rate

of 2000 rpm for 60 sec and dried at 90 °C for 30 min in the oven filled with N₂ gas. The thickness of ZnO layer as electron injection/transport layer was about 20 nm. The QDs were dispersed in CHB:o-DCB (volume ratio of 8:2) at a concentration of 10 mg mL⁻¹ to form the ink. All PMMA with different molecular weights (purchased from Sigma-Aldrich) were dissolved in the QD ink at a concentration of 1 mg mL⁻¹. The QD inks were printed in the sub-pixel using an UJ200 inkjet printer (Unijet Corporation) equipped with a Dimatix cartridge, followed by thermal annealing in a vacuum oven at 120 °C for 10 min to remove any residual solvent. Then HTLs CBP, MoO_x, and Al electrode were thermally evaporated under a vapor pressure of 1 × 10⁻⁶ torr onto printed QDs film. The deposition rates of each layers were 1 Ås⁻¹ for CBP sole layer. And then MoO_x, and Al were thermally evaporated with rate of 0.2 Ås⁻¹, and 4–5 Ås⁻¹, respectively.

2.2.2 Current-voltage-luminance Measurement

The current-voltage (I-V) characteristics were measured with a Keithley 236 source measurement unit, while the electroluminescence was measured with a calibrated Si photodiode (Hamamatsu, S5227-1010BQ) with a size of 10 mm × 10 mm placed at an angle normal to the device surface, assuming that the device was a Lambertian source. To detect a turn-on voltage of light-emitting diodes, we use an ARC PD438 photomultiplier tube (PMT) with the Keithley 236 source measurement unit. The electroluminescence (EL) spectra and the Commission Internationale de L'Eclairage (CIE) color coordinates

were measured with a Konica-Minolta CS-1000A spectroradiometer. The luminance and efficiency were calculated from the photocurrent signal of photodiode with a Keithley 2000 multimeter, and corrected precisely with the luminance from spectroradiometer (CS-2000).

The chromatic characteristics were calculated from EL spectra measured by the CS-1000A spectrometer using the CIE 1931 color expression system. The tristimulus values XYZ can be calculated by following equations,

$$X = K_m \int_0^{\infty} \bar{x}(\lambda)P(\lambda)d\lambda \quad (2.1)$$

$$Y = K_m \int_0^{\infty} \bar{y}(\lambda)P(\lambda)d\lambda \quad (2.2)$$

$$Z = K_m \int_0^{\infty} \bar{z}(\lambda)P(\lambda)d\lambda \quad (2.3)$$

where, $P(\lambda)$ is a given spectral power distribution of emissive source, \bar{x} , \bar{y} and \bar{z} are the CIE standard color matching functions (see Figure 2.2) and K_m is the weighing constant (683 lm W^{-1}). From the tristimulus values, the CIE color coordinates calculated by following equations,

$$x = \frac{X}{X+Y+Z} \quad (2.4)$$

$$y = \frac{Y}{X+Y+Z} \quad (2.5)$$

$$z = \frac{Z}{X+Y+Z} \quad (2.6)$$

Any color can be plotted on the CIE chromaticity diagram.

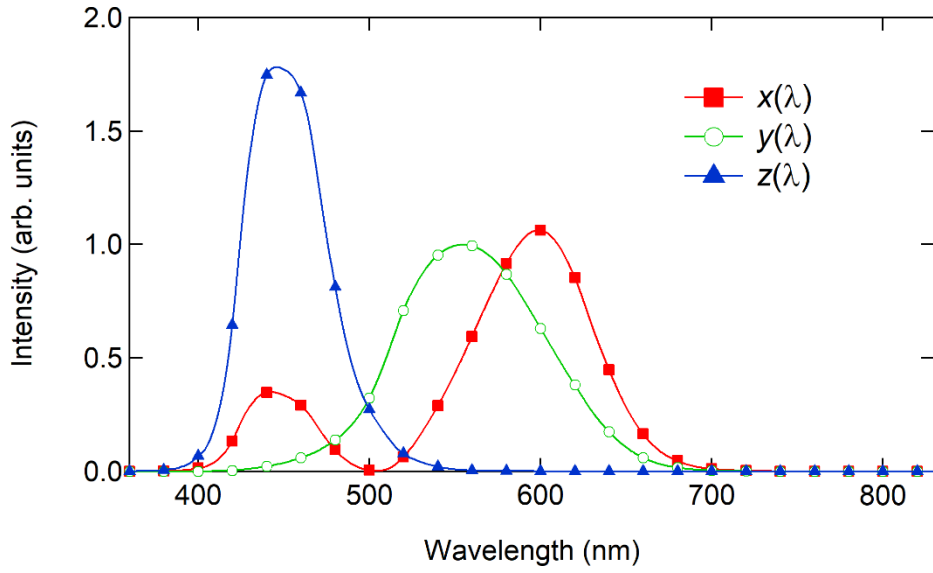


Figure 2.3 The CIE standard observer color matching functions

2.2.3 Efficiency Calculation Methods

To evaluate the emission properties of light-emitting diodes, the commonly employed efficiencies are the EQE, the current efficiency (C.E.) and the power efficiency (P.E.).

The external quantum efficiency can be defined by the following equation.

$$\text{EQE} = \frac{\text{number of emitted photons}}{\text{number of injected electrons}} (\%)$$

Typically, QLEDs or OLEDs emit light into the half plane due to the metal contact. Without any modification for increasing out-coupling efficiency, over 80% of the emission can be lost to internal absorption and wave-guiding in a simple planar light-emitting device.

Since human eye has different spectral sensitivity in visible area, the response of the eye is standardized by the CIE in 1924 (see \bar{y} in Figure 2.3). The luminous efficiency weighs all emitted photons according to the photopic response of human eye. The difference is that EQE. weighs all emitted photons equally. C.E. can be expressed by the following equation.

$$\text{C. E.} = \frac{\text{luminance}}{\text{current density}} (\text{cd A}^{-1})$$

The luminance value (cd m^{-2}) can be easily measured by the commercial luminance meter (CS-1000A in this thesis).

The power efficiency is the ratio of the lumen output to the input electrical power as follows,

$$\text{P. E.} = \frac{\text{luminous flux}}{\text{electrical power}} (\text{lm W}^{-1})$$

The EQEs can be useful to understand the fundamental physics for light emission mechanism, while the PEs can be useful to interpret the power dissipated in a light-emitting device when used in a display application.

2.2.4 Other Characterization Methods

Absorption and photoluminescence: The absorption spectra were measured using a UV–Vis spectrometer (Cary 5000, Agilent) and the PL spectra were measured using a spectrometer (SpectraPro 2150i, ACTON) and a Xenon lamp. In case of solution, materials were dissolved in toluene or solvent mixture (CHB:DCB = 8:2). Time-resolved PL was obtained from a time-correlated single photon counting system (Horiba–Jovin Yvon) consisting of avalanche photodiodes (timing resolution of 350 ps) and a multi-channel analyzer (HydraHarp, Picoquant).

Film Thickness Measurement: Ellipsometers (Elli-SE-UaM8, Ellipsotechnology) and an AFM (XE-100, Park Systems) were used for measuring the thicknesses of films. The cross-sectional TEM images were obtained at 200 kV using a JEM-2100F HR TEM (JEOL).

Rheological parameter measurement: The contact angle and viscosity of the QD droplets were measured using a Phoenix 300 contact angle analyzer (SEO) and a μ VISC viscometer (Rheosense), respectively.

Film profile measurement: Optical profile images were obtained using a ZeGage optical profilometer (WizOptics)

2.3 Theory

2.3.1 Surface Energy Analysis

Surface energy of liquid can be calculated from the contact angles. The shape of dropped liquid droplet on solid surface is influenced by three parameters; solid-liquid interfacial tension, Γ_{SL} , solid-vapor interfacial tension, Γ_{SV} , and liquid-vapor interfacial tension, Γ_{LV} .

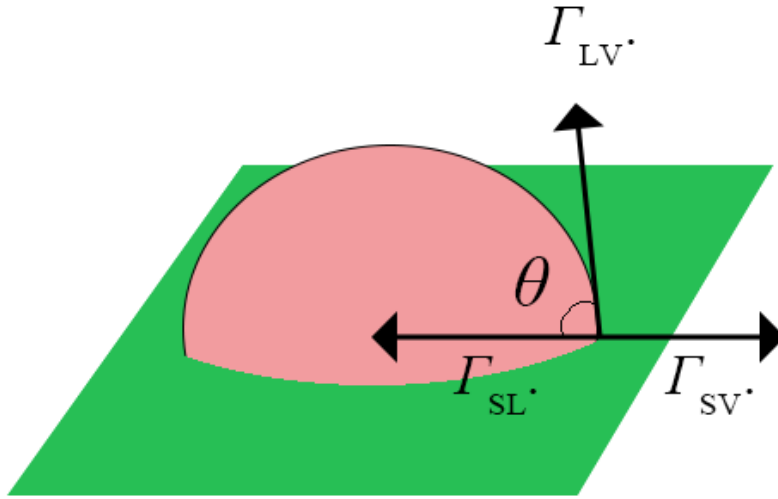


Figure 2.4 Description of surface tension

Young's equation describes the relationship between surface energy of materials by following equation.

$$-\Gamma_{SV} + \Gamma_{SL} + \Gamma_{LV} \cos \theta = 0 \quad (2.9)$$

Owens and Wendt model introduced surface energy by the sum of dispersive component (as known as non-polar component), and polar component [24].

$$\Gamma_s = \Gamma_s^d + \Gamma_s^p \quad (2.10)$$

where Γ_s is surface energy, Γ_s^d is dispersive component, Γ_s^p is polar component.

The relationship between surface tension components and contact angle also shown as following equation.

$$\Gamma_L(1 + \cos \theta) = 2\sqrt{\Gamma_s^d}\sqrt{\Gamma_L^d} + 2\sqrt{\Gamma_s^p}\sqrt{\Gamma_L^p} \quad (2.11)$$

where Γ_L , Γ_L^d , and Γ_L^p are surface energies of test liquid.

Two contact angles of different liquids, which are a polar liquid and a non-polar liquid, are needed to calculate dispersive and polar component of surface energy. By solving these equations, surface energy of solid substrate can be obtained

In this thesis, deionized (DI) water and diiodomethane (CH_2I_2) was used as a polar liquid and a non-polar liquid, respectively.

2.3.2 Coffee Ring Effect and Capillary Flow

In the drying drops, non-uniform films are easily formed because the tendency for solute to segregate at the edge during the evaporation. This is well known as coffee ring effect which leads a ring-like deposit near the periphery. It originated from the coffee residue is generally concentrated along the border of the stain, making the sediment like a ring when the coffee dries. The reason of coffee ring effect is because of inhomogeneous flow that replenish the solution from the center to the edge by a difference in evaporation rates by surface area at the center and edge in the drying drops. In general, this outward flow is called as capillary flow or laminar flow when there is a coffee ring effect. In the inkjet technology, coffee ring effect usually occurs when solute particles in the ink accumulate along the periphery of the droplet during drying because of inhomogeneous evaporation of the solvents. The resulting uneven morphology could occur electric defects in the device.

2.3.3 Marangoni Flow

When there is surface tension gradient, the solvent of the higher surface tension region pulls the solvent of the lower surface tension at surface of drops. This surface tension gradient usually drives a convective flow, called Marangoni flow, inside the liquid. The application of Marangoni flow has existed in many fields including heat-mass transfer, production of materials, and surface coating. Gradient in surface tension can be caused by local temperature variation, surfactant which the lower surface tension, or solvent mixture [25-35]. Uneven evaporation draws energy unevenly from the drop, creating a temperature gradient, which in turn changes surface tension. This result is both surprising and significant, since Marangoni flow directed radially inward along the substrate actively hinders the deposition of particles at the drop edge [32,35]. The local gradient of the concentration of a substance may drive the Marangoni flow inward if a substance that lowers the surface tension of the liquid is added to the droplet. Accumulation of surfactants near the edges could produce a Marangoni flow in the opposite direction to the external flow which suppress the capillary flow [26,28,33]. Solvent mixture uses different surface tension of solvents at high and low boiling points. Solvents with low boiling points and low surface tension evaporate faster at the contact line, leaving high boiling points and high surface tension solvents. This results in surface tension gradients, and the resulting flow circulate the entire ink, making a uniform film formation [36,29,34].

Chapter 3

Printing Accuracy Improvement of Inkjet printed QLEDs with Engineered Bank using Highly Fluorinated Photopolymer

3.1 Introduction

Considerable effort has been devoted to improving the device efficiency and operational stability of the inkjet printed QLEDs. In contrast, little attention has been paid to be the structure design of the inkjet-printed QLEDs, and most of the endeavors have been dedicated to spreading and wetting property of QD droplets. The printing accuracy of inkjet printing is relating to way of controlling the ink droplet fall from nozzle to proper position of the active area, and it is relation with the angular deviation of the droplet leaving the printer

nozzle [37]. The angle deflection of droplet may be caused by nozzle clogging, machine tremor and error occurrence in inkjet-printing machine, and it leads to two problem such as mis-aiming and overflow. Figure 3.1 shows the concept art of printing failure in case of inelastic collision by satellite drop. By a variety of external environmental factors, the printing failure may be inevitable. The effort to compensate printing failure also have been conducted.

V. V. Khatavkar et al. reported to need hydrophobic wall preventing from overflow out of the bank using a fluid dynamic study [38]. T.-M. Liou et al. showed to require a proper surface energy of wall for forming a flat film in the bank using computational fluid dynamics (CFD) [39]. D. Y. Kim et al. fabricated an inkjet printed QD film to color conversion layer using self-assembly monolayer (SAM) treatment in recent [40]. But SAM treatment process is inefficient way because it has reliability problem in large area and is difficult to apply the manufacture line in display area.

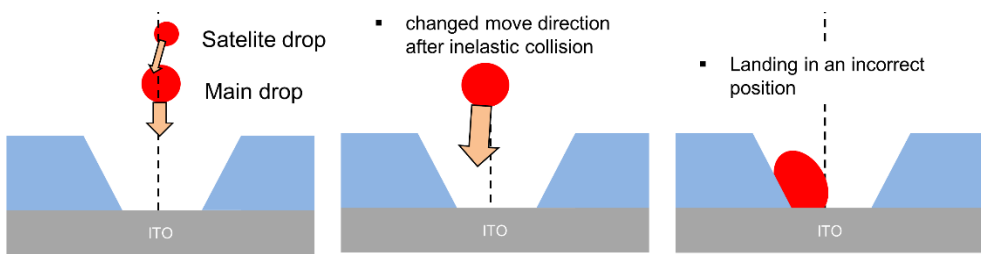


Figure 3.1 (left – right) Schematic of mechanism of mis-aiming, which means droplet landing in an incorrect position

Despite the implications of these previous studies, there is a lack of research to use a fluorinated photo-reactive polymer in single process fabricating bank structure. Although they are conceptually simple, such studies are complicated because the control of solubility of fluorinated developer solvent is difficult in case of general fluorinated photopolymer. This solubility problem comes from material design for photo-response. There are reports to use photoresist using the fluorinated polymer. Nelson Felix et al. [41] reported a polymer photoresist based on the depolymerization of acetal linkage using acid generated from general PAG. But the presence of PAG leads to a solubility problem not dissolving fluorinated developer solution. E. Reichmanis et al. [42] introduced the polymer photoresist by copolymer of trimethylsilyl methacrylate and 3-oximino-2-butanone methacrylate, using increased solubility in cyclohexane developer due to main-chain scission by deep-UV irradiation. The idea regarding the polymer main-chain by this oxime linkage and monomers that can occur beta scission derives from the previous report.

To minimize the solubility issue, I used novel P(FOMA-BMOMA-IBMA) PFBI using the beta scission concept reported for nice solubility in fluorinated developer solvent [22]. I evaluated a photo-responsive property and resistance to printing failure of this material. Thus, I demonstrated that simple but good printing accuracy by engineered bank using novel PFBI-1 can be used to fabricate inkjet printed Quantum dot light emitting diodes and, consequently,

the performance of the resulting electroluminescent devices for display, lighting, or laser applications.

3.2 Evaluation of Pixelated Structure with PFBI

The concept art of compensation for printing failure of is illustrated in Figure 3.2. Even if a drop in a drop with angle deviation falls, it can roll down to the active area if it has low surface energy not only in the top area but also in the wall. A bank with low surface energy in roof and wall must be created in single process rather than complicated process with different surface energies of roofs and walls. However, such studies are complicated because the control of solubility of fluororous develop solvent is difficult in case of general fluorinated photopolymer. The generally using PAG to photoresist material leads to a solubility problem not dissolving fluororous develop solution. The polymer photoresist by copolymer of trimethylsilyl methacrylate and 3-oximino-2-butanone methacrylate, using increased solubility in cyclohexane developer due to main-chain scission by deep-UV irradiation.

In this study, I used novel P(FOMA-BMOMA-IBMA) PFBI using the beta scission concept such as oxime linkage cleavage reported for good solubility in fluororous solvent [22]. A detailed explanation of material synthesis and property is described in the literature. The material contains fluorine, which has very low surface energy. This hydrophobic property of PFBI can

prevent from mis-aiming and overflow out of the bank. These excellent properties allow the resistance to the printing failure and enable to inkjet-printed QLEDs.

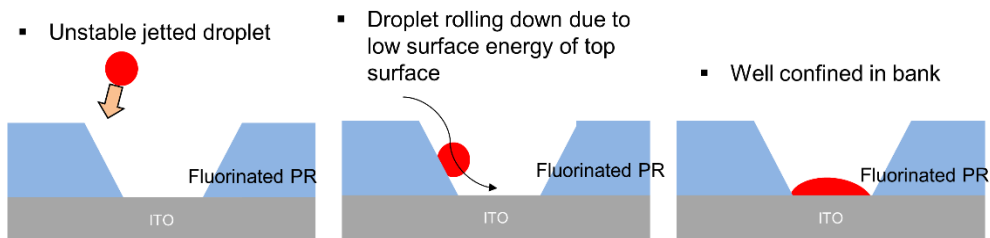


Figure 3.2 (left – right) Concept art of compensation for printing failure such as mis-aiming and overflow

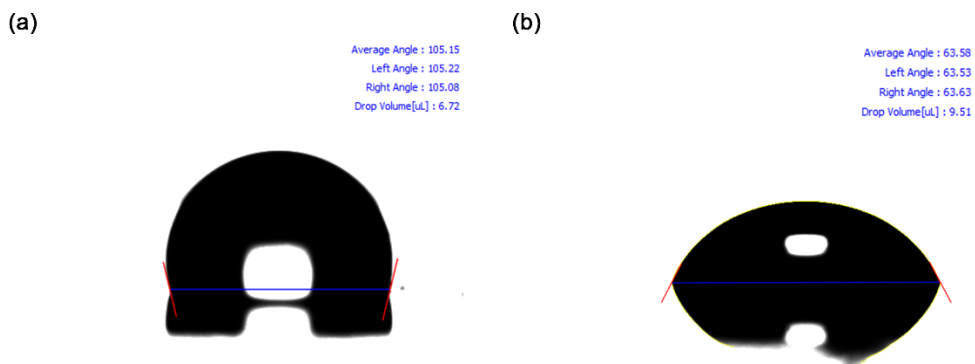


Figure 3.3 Photography of (a) deionized water and (b) diiodomethane droplets on top of PFBI for measuring the contact angles between droplet and thin films; Calculated surface energy is 17.5 mJ m^{-2} by Owens and Wendt model.

3.2.1 Highly Fluorinated Photopolymer, PFBI for Inkjet-printed QLEDs

Orthogonal processing using hydrofluoroether-based solvents with hydrophobic and fluorophilic properties is mainly directed to fabricating resist patterns by reducing the solubility to the solvent. In order to solve this problem, a deprotected phenolic resist can be removed by adding a small amount of isopropyl alcohol or hexamethyldisilazane (HMDS) in the fluorous solvent. Therefore, the development of highly fluorinated photoresist that can be patterned with no additives such as photoacid generator (PAG), and that is capable of producing a pattern due to increased solubility in a fluorous solvent after UV irradiation is necessary.

A novel P(FOMA-BMOMA-IBMA) PFBI is made by copolymerization of perfluorooctyl methacrylate (FOMA) with benzil monooxime methacrylate (BMOMA) and isobornyl methacrylate (IBMA). Measurement of surface energy of this material are required to determine the potential to avoid printing failure. An easy way to check surface energy of films is to measure the contact angle of the polar solvent (deionized water) and non-polar solvent (diiodomethane) on that as in Figure 3.3. The measured contact angle is 105.15° for deionized water and 63.58° for diiodomethane. By substituting the contact angle is in the Good Van Oss model (Eq. 2.11), we were able to extract the surface energy of the film be expressed as Section 2.3.1. The average surface energy of layer is 17.5 mJ m^{-2} by Owens and Wendt model. It is noteworthy

that the surface energy of PFBI can be feasible to the droplet rolling down to the active area though unstable jetting.

3.2.2 Characteristics of Pixelated Structure made of PFBI

Identifying the shape of the bank structure is necessary to increase the reliability of future experiments. To fabricate the PFBI bank, a 20 wt/vol% PFBI solution in PF-7600 was spin-coated on ZnO/ITO/glass substrate (500 rpm for 10 s, increase to 1000 rpm and stand rpm for 50 s) and baked it at 80 °C for 3 min. UV-irradiation was performed with 2.3 J cm⁻² by MA6 aligner and the irradiated substrate was dipped into HFE-7300 for 7 min and rinsed with FC-770. Figure 3.4 shows images of pixelated structure using PFBI photopolymer. Optical microscope image shows the contrast of bank and scale of bank design in figure 3.4a. SEM image and optical profiler images shows the real thickness of polymer bank and the accurate profile in figure 3.4b-c. It is noteworthy that the profile of pixelated structure using PFBI has enough sidewall angles by roll-down of the ink droplet into active area. AFM images was investigated to check that there was no remained thin film with 1.84 nm of rms value which of ITO as shown in Figure 3.4d. To verify the presence of the remaining film after development process is important. It worse the wetting of ink droplet in active area and the performance of inkjet-printed QLEDs. Thus, our pixelated structure using PFBI have the potential to compensate the printing failure.

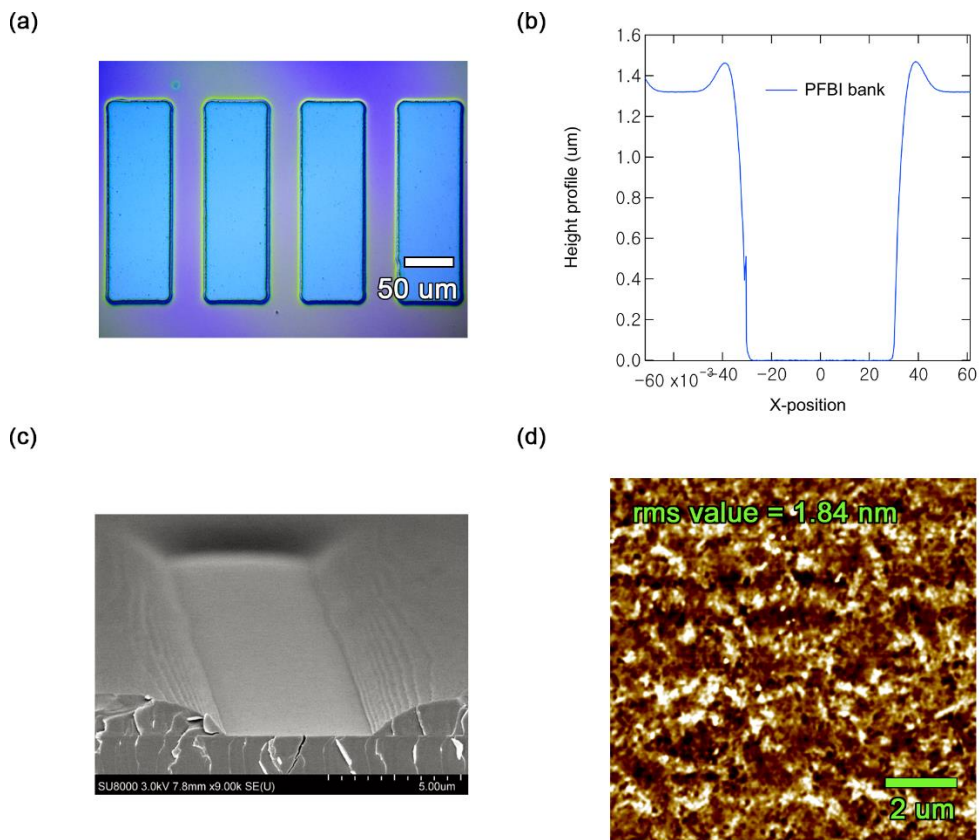


Figure 3.4 Well formation of bank structure. (a) Optical microscope image, (b) SEM image of cross-sectional bank. (c) AFM morphology image of active area after development of PFBI with 1.84 nm of rms value, (d) Profile image of cross-sectional bank indicating 1.5 μm of height.

Previous experiments have confirmed that the PFBI has 17.5 mJ m^{-2} of low surface energy. This will compensate for the printing failure such as mis-aiming and overflow. Therefore, they want to assess whether a wrong drop can roll along a phobic surface into an active area, and also to ensure that overflows

are prevented when a solution of the same volume is jetted to a structure of the same height.

Confining of ink droplet into active area is important to form film to desired thickness. If an unstable dispensing of the droplets leaves the desired position, the active area cannot be controlled by the desired volume. If the droplet collides with a surface with sufficiently little surface energy and a surface with sufficiently low side angles, the droplet may be able to move into the active area. To prove this, we conducted an experiment to verify that the actual jets can enter the active zone after a collision at that point. Figure 3.5 shows an image of the ink printed on the PFBI bank which the bright part is the surface of the ITO and the dark part is the top surface of the PFBI film. The bright sky-blue dotted line indicates where the actual active area exists, while the red dotted line indicates a jet slightly off the bank. The droplets printed first from the left are jetted onto the ITO surface and spread by high surface energy. The second printed drop fell on the PFBI surface of the low surface energy and is less diffused than the first printed droplet. The part with the third and fourth droplets from the left is where the actual bank exists. These droplets are moved from the red dotted line to the sky-blue dotted line, showing that the droplets were moved through a green arrow in figure. These moved droplets mean they can compensate for errors such as Miss Aiming.

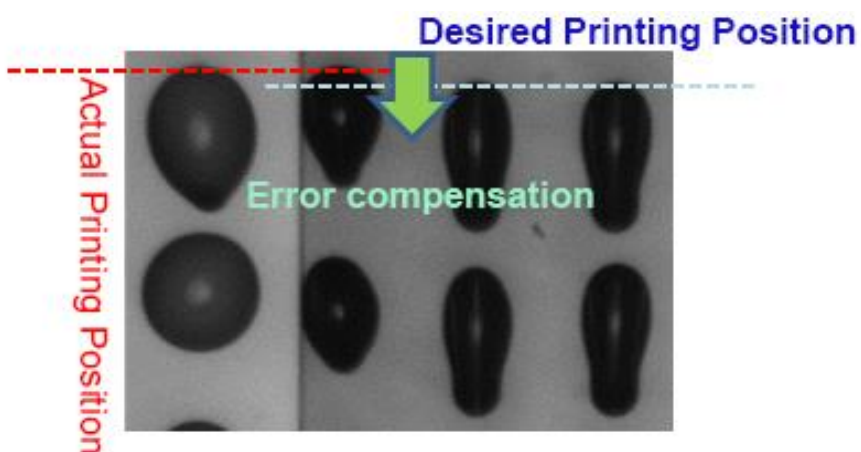


Figure 3.5 The droplet image of printed QD ink on PFBI substrate (right gray region) and ITO (left bright region). Red line is an actual printing position. Blue line is a desired printing position. Green arrow means compensation of Mis-aiming by hydrophobic property of PFBI.

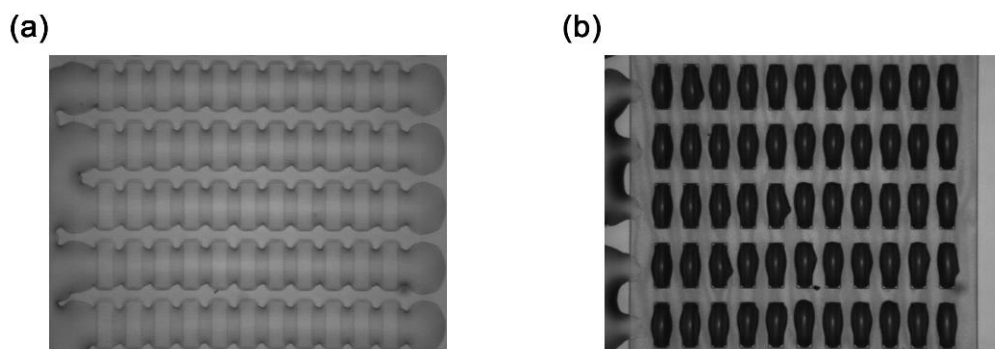


Figure 3.6 The droplet image of printed QD ink on (a) conventional PI bank and (b) PFBI bank. The hydrophobic property of PFBI prevents from the overflow of printed QD ink in same volume.

Preventing overflow in a bank is to maintain uniformity from external factors such as the deviation of the bank sidewall, the horizontal tilt of the substrate, or the change in the morphology on the film surface. If the surface of the bank has sufficiently small surface energy, it can be well confined within the bank due to high contact angles to ensure the same volume. To evaluate this, a substrate formed from polyimide film, which is generally used as a bank material, was prepared with fabricating the same thickness. Surface energy of PI is 56.71 mJ cm^{-3} , which is more than three times larger than the PFBI. The prepared substrates using PI and PFBI have a sub-pixel of $60 \text{ um} \times 180 \text{ um}$ and 1.4 um of height. The solution was prepared as a CHB:DCB mixture showing good efficiency recently and the volume of droplet was jetted to 20 pl , which is enough to overflow in PI film. Figure 3.6 shows the results of jetted droplets with the same volume on conventional PI and PFBI bank substrate. The hydrophobic property of PFBI-1 prevents from the overflow of printed QD ink in same volume as shown in figure.

These two results demonstrate that PFBI banks can fully compensate for printing failures. It is expected that the implementation of the device with this material will ensure uniformity and make a good performance.

3.3 Evaluation of QD Inks on Pixelated Structure with PFBI

Previous experiments have shown that CHB has a high boiling point and proper viscosity for high surface tension, making it easier to jet. However, it is necessary to select proper ink for a good solution for PFBI material to be implemented as a device. Figure 3.7 shows a photograph of a microscope using a solution from the CHB:DCB mixture in the PFBI bank. As shown in the figure, many contours are visible, which means a dome-shaped film is formed. If this is made into a device as it is, the electric field will not be properly distributed due to uneven thickness, which will lead to rapid device deterioration. The reason why film is formed is that due to the high angle of contact, the solute of the ink cannot accumulate around peripheral, causing the contact line to recess and eventually push back to the active area. Because a recessed solution into center was sufficiently concentrated, but the contact angle was still high due to low surface energy on the wall, it is resulting in the formation of film in this dome-shape form. Marangoni flow due to dual solvents is also working to strengthen this phenomenon. Therefore, we want to make a device by selecting a proper solution that can distribute films that are formed in the form of domes.

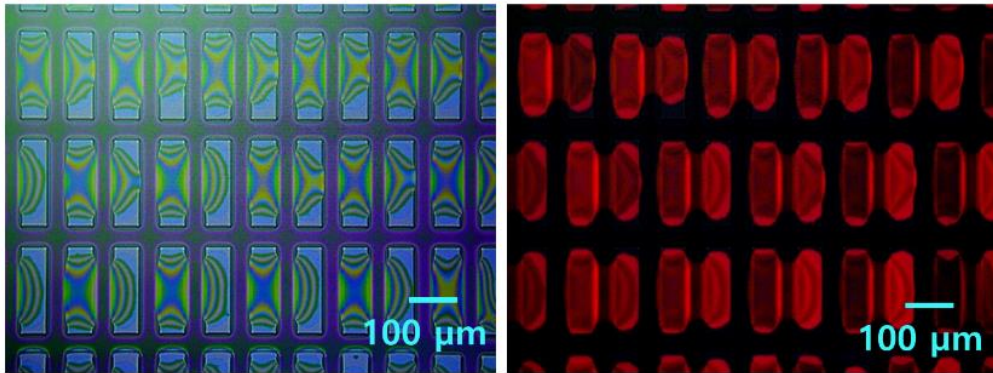


Figure 3.7 The droplet image of printed QD ink (dual solvent; CHB:DCB = 8:2) on PFBI bank; (left) optical microscope image; (right) Photoluminescence image.

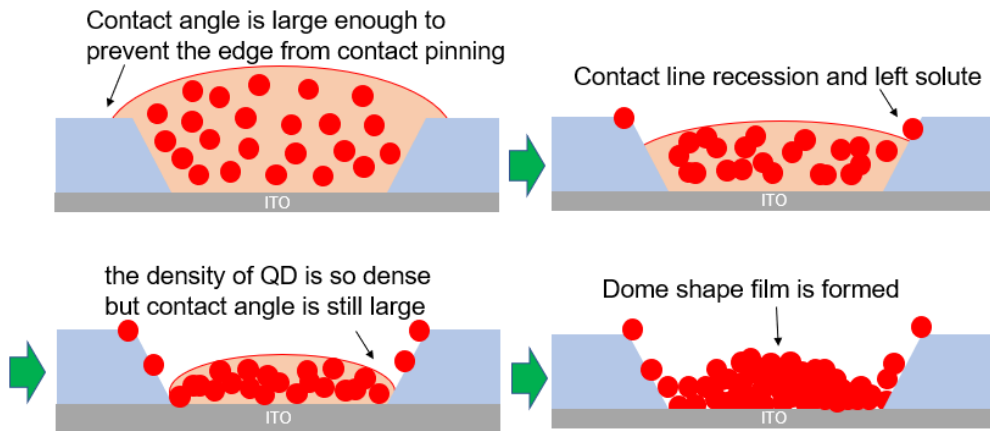


Figure 3.8 Scheme of how to be made the dome shape film formation

3.3.1 Morphology properties of QD ink on pixelated PFBI structure

Dual solvents in devices with inkjet-printed QLEDs typically cause Marangoni flow to be prevented from coffee ring. This becomes the direction in which the film formation in the dome form is strengthened in our experiments. Therefore, it is intended to reduce the formation of dome shapes by strengthening the capillary flow. Figure 3.8 shows scheme of how to be made the dome shape film formation of dual solvent ink on the hydrophobic surface of the bank.

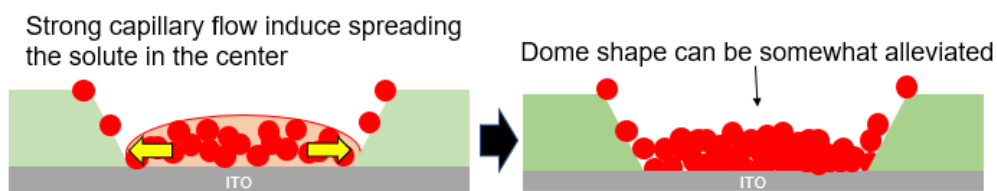


Figure 3.9 Scheme of how to alleviate the dome shape film formation

Figure 3.9 shows the idea of how to alleviate the dome shape film formation on the hydrophobic surface of the bank. We found a single solvent with a low viscosity and low surface tension that could cause a strong capillary flow. Low viscosity allows the solute to be pushed from the center to the periphery. Low surface tension can reduce the angle of dome form by lowering the angle of contact. In addition, there is one more requirement, and for printing, a single solvent must have a boiling point high enough to prevent nozzle clogging. Thus, isoparaffin was chosen because it has a low viscosity of 1.08

cPs and a relatively low surface tension of 25.44 mN m⁻¹. Also, it has a relatively high boiling point of 180 degrees, which makes it easy to jet. The material properties of dual solvents and isoparaffin are summarized in Table 3.1 below.

	Viscosity (cPs)	Surface tension (mN m ⁻¹)	Boiling point (°C)
Dual solvent (CHB:DCB)	2.8	33.16	CHB: 240 °C ^a DCB: 180 °C ^a
Isoparaffin	1.08 ^b	25.44 ^b	~180 °C ^a

Table 3.1. Material property such as viscosity, surface tension and boiling point of dual solvent and isoparaffin solvent, respectively; a) taken data from Merck and sigma Aldrich corporation; b) taken data from reference [41]

Figure 3.10 shows an image of an isoparaffin base quantum dot ink jetting to a PFBI substrate. To demonstrate that the quantum dot ink based on isoparaffin solvent is suitable, PFBI substrates are prepared which is same manufactured with the substrate of Figure 3.10 which have a sub-pixel of 60 um x 180 um and 1.4 um of height. The solution of QD ink was prepared as a isoparaffin and the volume of droplet was jetted to 20 pl. As shown in figure, the material property of isoparaffin such as low surface tension and viscosity can reduce forming dome shape of QD ink. However, the wetting is also bad and there is poor uniformity between pixel due to solution pulling in such direction. To solve this problem, a rectangular structure was constructed into

an oval. This is shown in Figure 3.11 through microscopic photographs and profile pictures. Figure 3.11a is an image taken immediately after printing and Figure 3.11b is an image printed and completely dried. Elliptical structures have solved the wetting problem to some extent and show that there is no significant pulling of solvent. Figure 3.11c is an enlarged microscope, showing that the center part still exist a convex part when magnified, even though the film appears to be well formed in Figure 3.11b. Figure 3.11d shows an image taken with surface profiler and shows convexity with nanometer thickness.

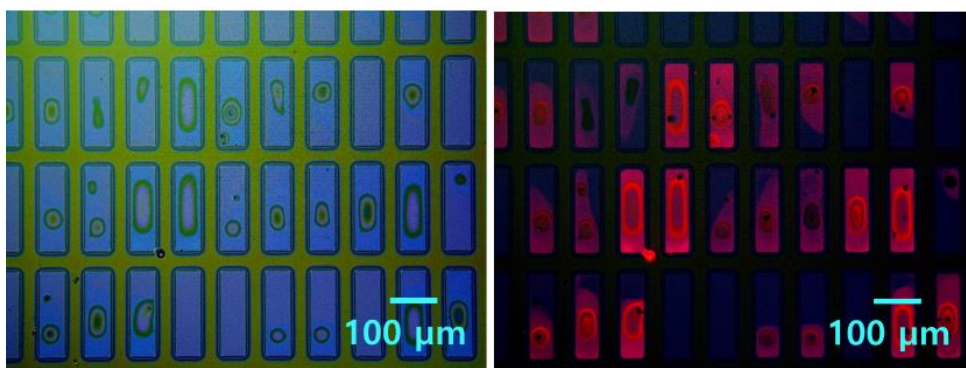


Figure 3.10 The droplet image of printed QD ink (single solvent; isoparaffine case) on PFBI bank; (left) optical microscope image; (right) Photoluminescence image.

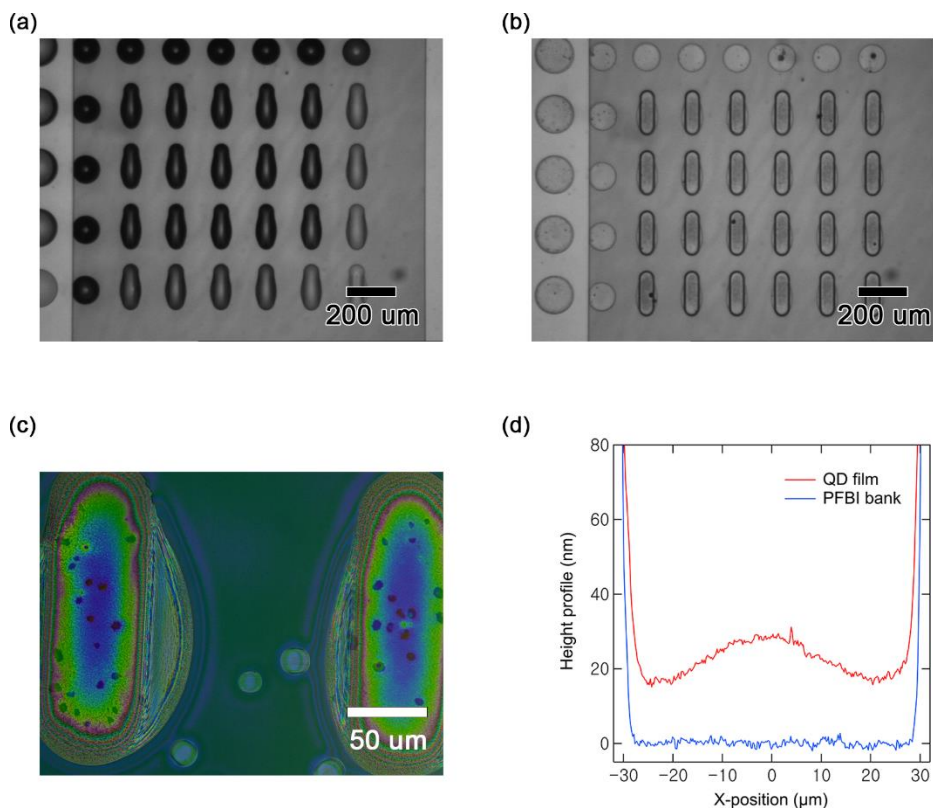


Figure 3.11 The droplet image of printed QD ink (single solvent; isoparaffin case) on PFBI-1 bank patterned by elliptical for ink wetting; (a) just printed; (b) dried; (c) optical microscope image; (d) profiler image;

3.3.2 Characteristics of inkjet-printed QLEDs using PFBI

Unlike OLED's EML materials, which are deposited by vacuum deposition, QD layers can only be fabricated using solution-based deposition techniques. [15] Generally, for patterning through inkjet printing, a bank for pixel definition is required. The bank is mainly used polyimide (PI), and low-

viscosity QD inks are used due to the nozzle clogging. Therefore, the volume of ink that must fit in a pixel is also very large, so the bank's height must be micrometer scale. However, since the ink solvent is generally hydrocarbons, [16] it is difficult to load a large volume of QD ink into the pixel because the difference in wettability between the lower semiconducting layers (ETL, HTL) and the PI banks is not large.

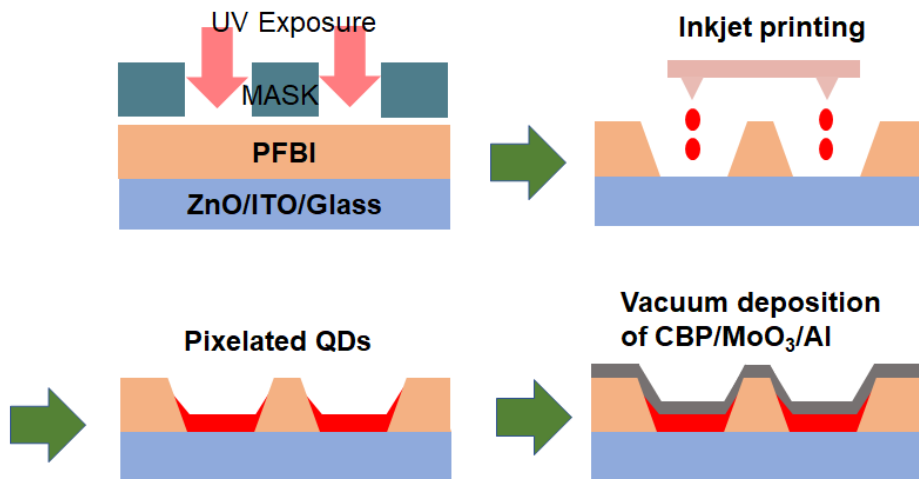


Figure 3.12 Fabrication process of inkjet printed QLED device using PFBI-1 bank.

(1) Development in fluoruous solvent. (2) Solvent drying. (3) Vacuum deposition of CBP, MoO₃ and Al; image is taken from reference [22]

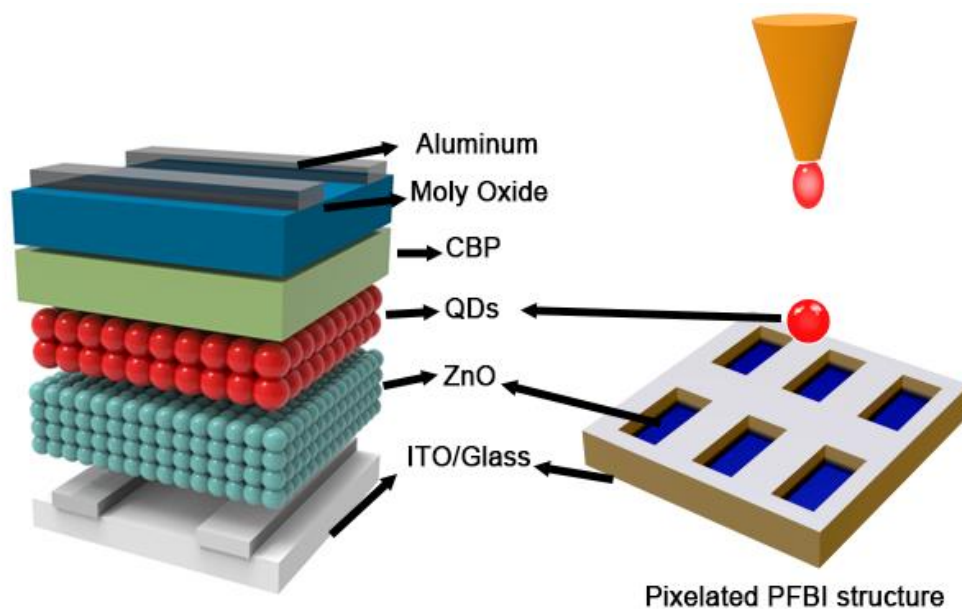


Figure 3.13 Schematic illustration of inverted structure of QLEDs and inkjet-printing on pixelated PFBI structure

Fig. 3.12 shows a fabrication process of photo-patterned QLED by depositing HTL CBP, MoO₃ and Al metal after red color emitting QD inkjet printing using PFBI-1 bank on top of ZnO layer. Figure 3.13 shows schematic illustration of inverted structure of QLEDs and inkjet-printed on pixelated PFBI structure. Isoparaffin-M (aliphatic hydrocarbons) was used as the ink solvent with broad boiling point. The concentration of the ink proceeded to 20 mg ml⁻¹. The size of the pixel is 60 x 180 μm and the thickness of the PFBI-1 pattern film is more than 1 μm. The pattern thickness of PFBI-1 measured using an surface profiler, was about 1.3 μm. After finishing the fabrication process, the performance of encapsulated QLED was evaluated.

Fig. 3.14 shows current density and luminance according to driving voltage. At 4 V, the current density was 39.0 mA cm⁻² and the maximum luminance was 5,300 cd m⁻². Fig. 3.10c shows the current density versus external quantum efficiency (E.Q.E.). The maximum E.Q.E. was as low as 0.11%, but I believe it can be further improved through elaborate optimization. Finally, the electroluminescence spectrum of QLED showed a narrow emission peak with a maximum intensity of wavelength of 642 nm and a full width at half maximum (FWHM) of about 40 nm.

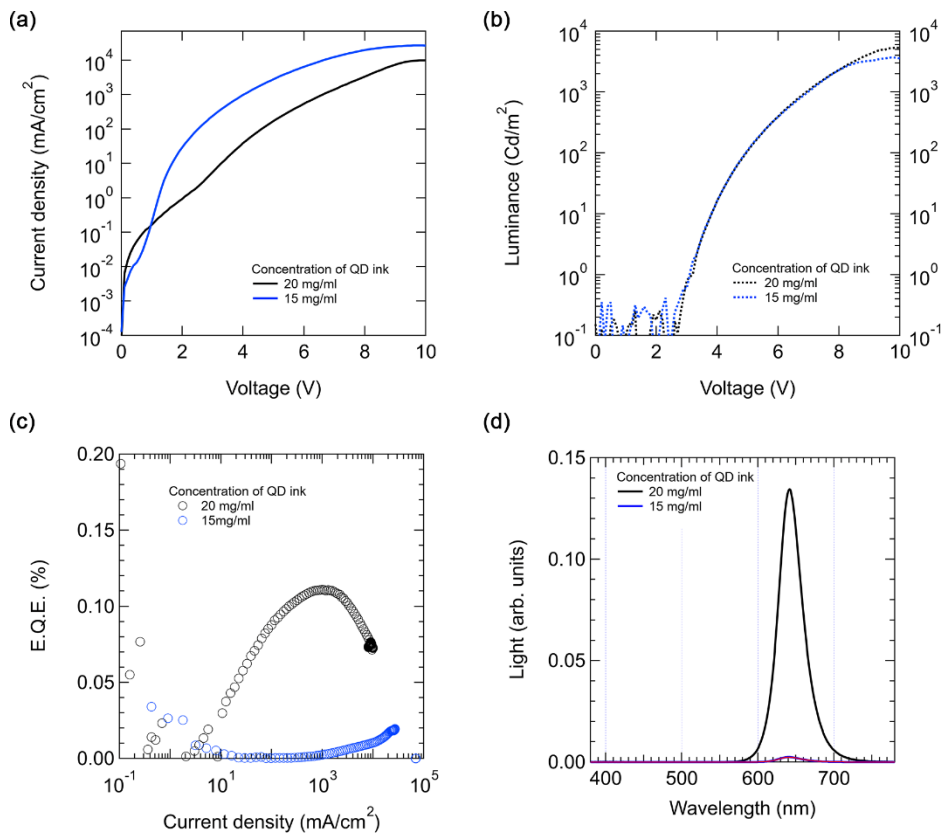


Figure 3.14 Electrical characteristics of inkjet printed QLEDs with PFBI-1 bank; (a) current density-voltage (J-V) characteristics: (b) luminance-voltage (L-V) characteristics: (c) EQEs versus the current density curve; (d) Electroluminescence spectrum.

3.4 Summary

In summary, we improved the printing accuracy against unstable inkjet-printed QD droplet and evaluated the electrical performance of inkjet printed QLEDs on the pixelated structure using highly fluorinated photopolymer, PFBI in single process. As a result, the QD-LEDs with PFBI showed well confined droplet in the bank and electrical performance of inkjet-printed QLEDs shows 4 V of operating voltage and 0.11% of maximum E.Q.E. was as low as 0.11 %. I believe it can be further improved through elaborate optimization like changing solvent of QD ink. The solvent combination of the solvent A, which is low boiling point & high surface tension, and the solvent B, which is high boiling point & low surface tension, can improve the device performance more. If $P_A < P_B$, where P_i is the vapor pressure of component i, and $\gamma_A > \gamma_B$, where γ_i is the surface tension of component i, then the relatively higher evaporation of component B tends to decrease the surface tension. In this case, the Marangoni flow will be induced from regions of low evaporation rate to regions of high evaporation rate.

Chapter 4

Efficiency Improvement of Inkjet Printed QLEDs Employing Polymer Additives

The efficiency of QLED devices by inkjet printing still fell short of the state-of-the-art level of QLED devices made by spin coating. One of the reasons is the bad roughness of the printed film by its inherent drying mechanism of solution. The uniformity of inkjet printing surface morphology has been thoroughly studied, with many reports examining improvements, especially focusing on coffee ring effects [43-45]. A widely used method alleviating coffee ring effect is to control the internal flow of droplets, via using fine-tuning viscosity of solution [46,34,47], chemical species additive [26-29,33],

and solvent mixture [48,36,49]. Inkjet-printed QLED by using binary co-solvent with different boiling point, cyclohexylbenzene (CHB) and 1,2-dichlorobenzene (o-DCB), firstly reported by Peng's group which exhibit the EQE of 1.1 % and maximum luminance (L) of 12,000 cd m⁻² [36]. Xiang et al. show the highest efficiency of inkjet-printed QLEDs in pixelated devices using red QD dissolved in a binary co-solvent, CHB and decane, which showed the EQE of 16.6 % and the maximum luminance over 10,000 cd m⁻².

Considerable effort has been devoted to improving the film uniformity and device efficiency of inkjet-printed QLEDs. The most endeavors have been dedicated to optimizing the printed droplet on flat substrate, but little attention has been paid to optimize the printed droplet on a pixelated structure. It is important to clearly define RGB subpixels of the QLED for fabricating QLED application in the industrial field. Uniformity of inkjet printed QD films in bank structures is much more difficult to control due to differences in surface characteristics between top, bottom and side surfaces of pixel-wise bank layers. The results show that inkjet-printed QLEDs with bank structures have overall lower performance than devices made of flat plates without bank structures [50-53]. Therefore, technology must be developed to improve the uniformity of inkjet printing QD layers within pixel banks.

In this study, we investigate how the performance characteristics of the inverted QLEDs produced using inkjet-printing technology are affected by the application of the QD-polymer composite in the emission layer. For the QD-polymer composite layer, we chose poly(methyl methacrylate) (PMMA) as a

chemical species additives, because of its low cost, high transparency, and easy blending with QD inks used in QLEDs. Firstly, we studied the optical profile of printed droplet on the plain substrate and morphology properties of the QD and QD–polymer composite films in the pixelated bank structure, by using optical microscopy, ZeGage profilometry and atomic force microscopy (AFM). In addition, the interface properties of the QD and QD–polymer composite thin films were analyzed using transmission electron microscopy (TEM). Secondly, we measured the performance of the inkjet-printed QLEDs and analyzed detailed electroluminescence (EL) images emitted from pixels. The approaches used for studying the inkjet-printed QD–polymer composite films in the pixelated bank structure and their application to QLEDs will be useful in studying the universal impact of inkjet-printing processed displays

4.1 Introduction of inkjet printed QLEDs

Quantum dot (QD) light-emitting diodes (QLEDs) are considered as a promising candidate for full-color displays due to their excellent color purity, wide color gamut, and cost-effective fabrication based on solution processes. In order to be used for quantum dots for next-generation displays, patterning method is important for achieving high resolution displays. Spin coating is a simple process that can be carried out using a solution type material, but it is impossible to pattern and difficult to apply to large area substrates. Considering expensive price of pure QDs, inkjet printing is the best candidate for fabricating QLED device with low materials waste.

In the inkjet printed QLED, there have been many attempts to eliminate bad morphology of printed film, which called coffee ring effect. They are divided into two ways to reduce coffee ring formation of ink droplet. One of methods is using Marangoni effect by solvent mixture, surfactant, and solute concentration. Some studies to reduce capillary flow by increasing viscosity has been also reported. The widely used method fabricating inkjet-printed QLEDs is solvent mixture method which use a mixed solvent with a different boiling point. However, the performance of devices fabricated in a pixelated structure are less than that of devices which not fabricated in a pixelated structure. Peng et al. reported inkjet-printed QLEDs with EQE of 1.1% and maximum brightness $12,000 \text{ cd m}^{-2}$ using solvent mixture consisting of CHB and 1, 2-dichlorobenzene (oDCB) [36]

However, the performance of devices fabricated in a pixelated structure are less than that of devices which not fabricated in a pixelated structure. The speculating reason for this is that, when using a solvent mixture, a low bp solvent was first dried, and then a high bp solvent is determined by the center morphology of inkjet printed dot which is equivalent to active area of the device. Figure 4.1 shows Schematics of the reason why inkjet printed QD films using dual solvent still have rough morphology in the case of pixelated device, leading to inferior performance of full device. After the droplet impacts the substrate, Marangoni flow initially exists in internal drops. After the film is formed to some extent, the low boiling point solvent will fly away and only the high boiling point solvent will remain. In that state, the same form of internal flow exists as for single solvents. At the end of drying, the high boiling point material determines the morphology of film with coffee ring effect, so the performance of the device is poor. On the other hand, non-pixelated inkjet printed QLED devices show relatively high efficiency [50,53]. Figure 4.2 shows schematics of the reason why inkjet printed QD films using dual solvent have better morphology in the case of non-pixelated device, leading to relatively good performance of full device; the solvent of high boiling point is expelled from center to edge of films. So, the whole film will be uniform unlike the pixelated device. Additional methods are needed to reduce the effect of film formation from pixelated elements to single solvents. It may be a good way to add polymer into solvent mixture, in order to generate additional Marangoni flow by polymer and be weaken capillary flow and.

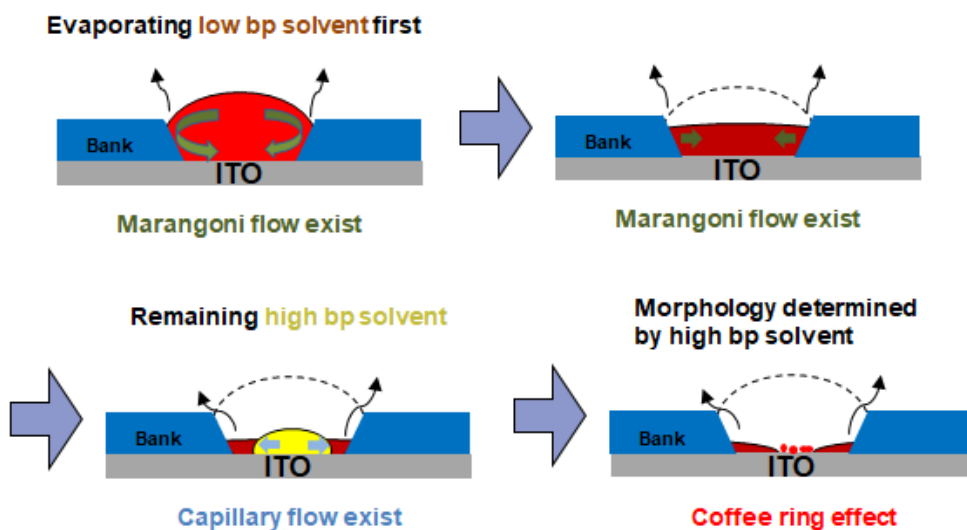


Figure 4.1 Schematics of the reason why inkjet printed QD films using dual solvent still have rough morphology in the case of pixelated device, leading to inferior performance of full device.

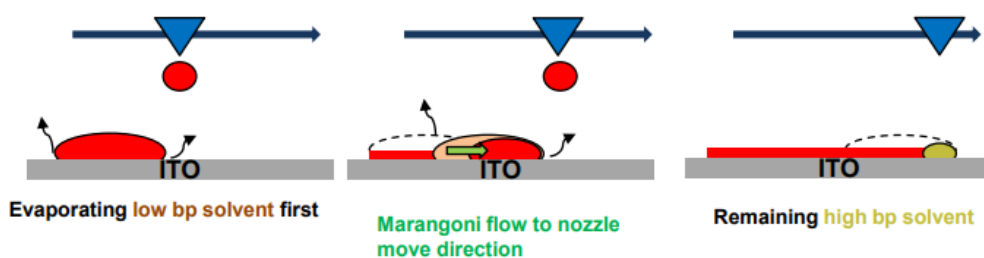


Figure 4.2 Schematics of the reason why inkjet printed QD films using dual solvent have better morphology in the case of non-pixelated device, leading to relatively good performance of full device; the solvent of high boiling point is expelled from center to edge of films.

4.2 Evaluation of QD-PMMA Composite Ink on Planar Substrate

4.2.1 QD-PMMA Composite Ink for Reducing Coffee Ring Effect

The internal flow dynamics can be changed by controlling rheological parameter. When polymer is added to a solution, surface tension and viscosity of the solution change. We thus added polymer, PMMA, into the QD solution, because of its optical transparency in visible spectra and easy blending for QD ink. In addition, there have been many papers using nanocomposites which often used to passivate of defect of quantum dot [54-56]. It can also reduce the voids in printed QDs that may arise leakage current and serve as electron blocking layer [57].

Since it is most important to identify the properties of the mixture, we first compared the properties of the general solution and the mixed solution. I prepared two types of QD inks by dispersing Red CdSe/Zn_xCd_{1-x}S QDs (630 nm) with 16 nm of diameter dissolved in co-solvent (CHB:o-DCB; a volume ratio of 8:2) without and with PMMA. In order to check the change in mole weight, a mixture solution with different mole weight of PMMA was also prepared such as pristine, 2 kDa, 8 kDa, and 350 kDa. For comparison, concentration of QD and that of PMMA in mixture is fixed at 10 mg mL⁻¹ and 1 mg mL⁻¹.

To find out how optical properties changed, the UV-Vis absorption spectra, photoluminescence (PL) spectra, and time-resolved PL (TRPL)

dynamics were compared with solutions, as shown in Figure 4.3. As a result, it shows little difference across samples in the UV–Vis absorption spectra, PL spectra, and the time-resolved PL decay time though different Mw of PMMA. Such a small change in optical properties may be the small amount of PMMA to change optical properties of solution and the quantum dots have less defects [56].

To do jetting the ink, it is important to understand how well the jetting works using an appropriate drop at the nozzle. In the field of inkjet technology, particular parameters were introduced to identify the ink jettability which is determined by rheological parameters such as viscosity, inertial force, and surface tension. The characteristics parameters, the Reynolds number Re , the Weber number We , and the inverse Ohnesorge number Z , defined as,

$$Re = \frac{\rho v l}{\eta} \quad (4.1)$$

$$We = \frac{\rho v^2 l}{\gamma} \quad (4.2)$$

$$Z = \frac{1}{Oh} = \frac{Re}{\sqrt{We}} = \frac{\sqrt{\rho v l}}{\eta} \quad (4.3)$$

where ρ , η , and γ are the density, viscosity and surface tension of the inks, respectively, l is the drop diameter, and v is the velocity of the drop. For a stable drop, the Z value needs to be in the range of $1 < Z < 10$ formation in the inkjet technology [58].

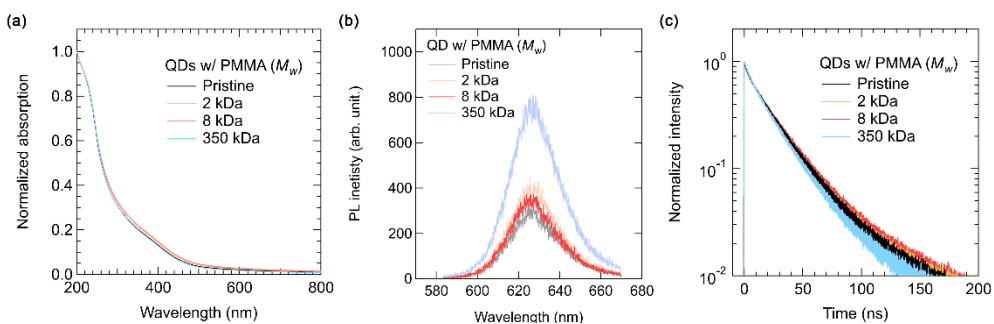


Figure 4.3 (a) Absorbance, (b) PL spectrum, and (c) Transient PL of pristine QD ink and QD + PMMA inks (M_w : 2 kDa, 8 kDa, and 350 kDa, respectively).

Figure 4.4 shows the contact angles of the pristine QD ink and the QD–polymer composite inks which are slightly lower compared to that of the former. The measured viscosity value of the pristine QD ink was 2.87 cP while those for the QD–polymer composite inks were marginally increased to 3.06, 3.00, and 3.16 cP, for PMMA molecular weight of 2 kDa, 8 kDa, and 350 kDa, respectively. These rheological parameters are summarized in table 4.1. In this experimental, the drop diameters and the droplet velocities of printed ink were 18.0–19.4 μm and 3.3–4 m s^{-1} , respectively.

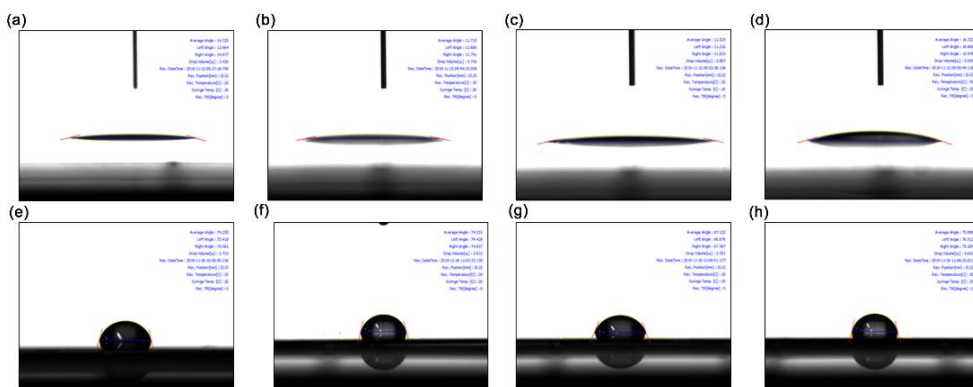


Figure 4.4 Measurement of contact angle of QD ink without and with PMMA varying the molecular weight of PMMA on (upper) silicon substrate and (lower) SAM treated substrate; (left to right) pristine QD ink and QD + PMMA inks (M_w : 2 kDa, 8 kDa, and 350 kDa, respectively).

	Density (kg m^{-3})	Viscosity (cPs)	CA on Si (degree)	CA on FOTS (degree)
Pristine	972	2.8	14.3°	74.2°
2 kDa	982	3	11.7°	74.5°
8 kDa	982	3	11.5°	67.1°
350 kDa	982	3.2	14.3°	72.7°

Table 4.1. Rheological parameter of QD inks without and with PMMA varying the molecular weight of PMMA

Using these rheological parameters of QD inks, the jettability window can exhibit using the characteristics parameters such as Re , We , and Z . The most common jettability window, $We-Re$ plot, is described to confirm that all the QD

inks exist in the printable range where appropriate single drop can be jetted. And that means $6.3 < Z < 8.9$ regardless of the PMMA M_w .

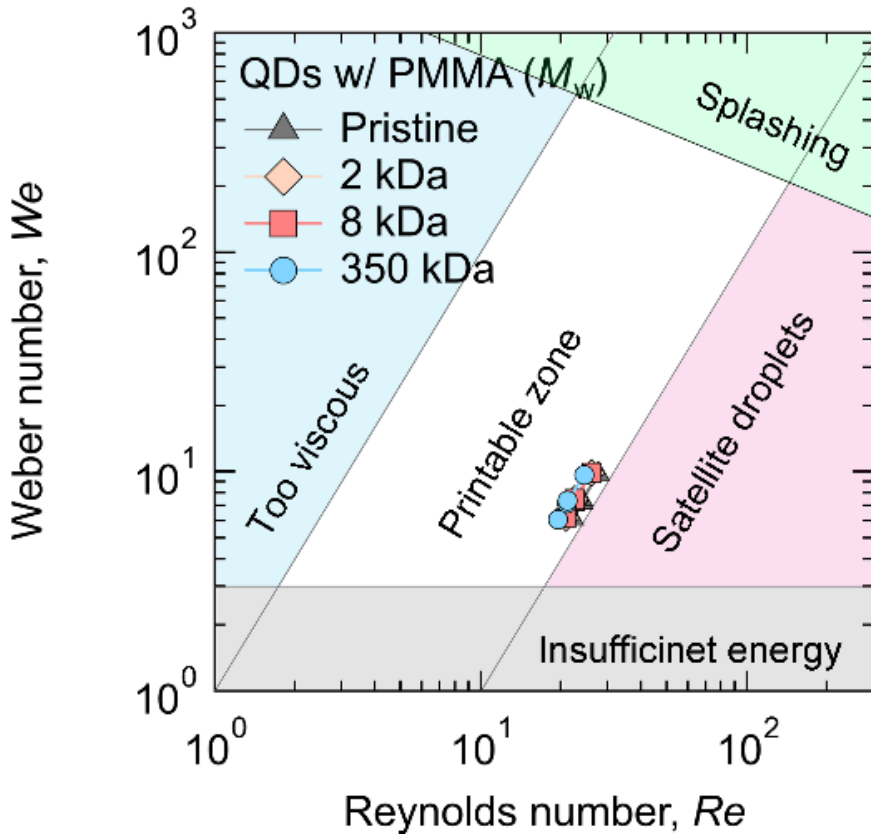


Figure 4.5 Weber number vs. Reynolds numbers of the pristine QD inks and the QD–PMMA (M_w of 2, 8, and 350 kDa) composite inks, indicating that all the inks are in the printable zone

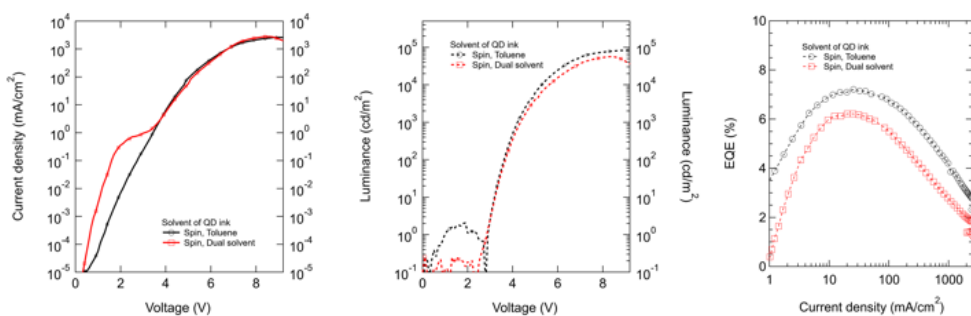


Figure 4.6 Electrical performance comparison of QD solution dissolved in (black) toluene and (red) CHB : DCB = 8 : 2 mixture in case of spin-coated QLEDs.

4.2.2 Morphology Uniformity of QD Droplet Film using PMMA Additives

To see if there is a Marangoni flow enhancement and surface smoothing effect, we first conducted an experiment with a single solvent. Unlike dual solvents, the additional effects of PMMA can be clearly confirmed when using single solvents. Since the device we are implementing is an inverted structure, we have jetted the corresponding ink onto the ZnO nanoparticles. Figure 4.7 shows photoluminescent image on ZnO NP films with pristine QD ink and QD-PMMA composite ink. Quantum dot-polymer composite ink selects one of the molecular weights of prepared polymers to 8 kDa. In Figure 4.7a, the surface energy of ZnO film is large enough, so the felt droplet with a single solvent spreads the surface and has a large-sized thin film. On the other hand, in the case of ink with polymer additives, the spread after impact is large, but it is shown in Figure 4.7b that the film is reduced from the initial size and

formed. It means that the contact line of droplet is recessed by polymer Marangoni flow, compared to its initial position which spreading solvent after impact.

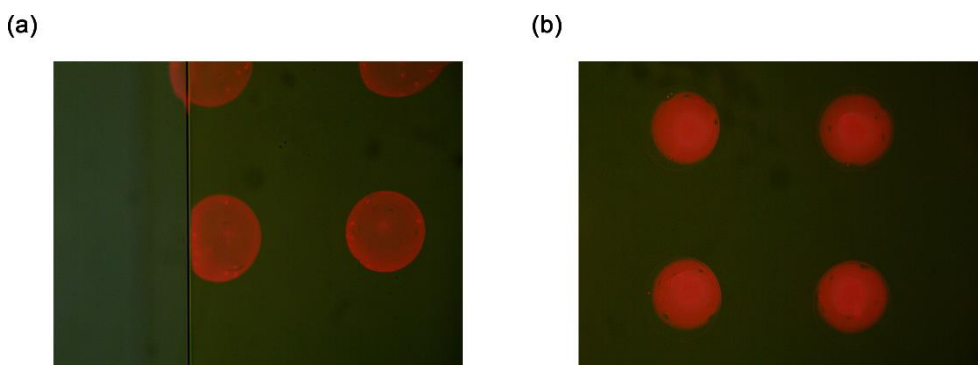


Figure 4.7 Photoluminescent image of printed QD droplets on ZnO NPs film induced by the 360 nm laser with (a) Pristine QD ink and (b) QD - PMMA composite inks (M_w : 8 kDa).

Figure 4.8a and 4.8b show the cross-sectional and 3D profiles of each droplet of the pristine QDs ink and that with the QD-PMMA (8 kDa) composite ink, respectively. They were inkjet-printed on a ZnO nanoparticles (NPs) layer and the ink volumes for them were 39 pL and 43 pL, respectively. As shown in Figure 4.8b, the droplet of the QD ink without PMMA showed an empty center area; the height of both side areas reached 10 nm while that of the center area was considerably lower as 1–2 nm, similar to a coffee-ring effect. On the contrary, when the QD- polymer composite ink was used, the spatial uniformity in the droplet was largely enhanced and it can be seen that both side and center areas are filled with the QD-PMMA composite with a

height of 15–17 nm. Interestingly, we found that the diameter of the droplet from the QD– polymer composite ink ($\sim 230 \mu\text{m}$) is slightly smaller than that from the pristine QD ink ($\sim 250 \mu\text{m}$) in spite of the larger ink volume.

To investigate the reasons, we observed the drying process of each droplet over time, as shown in Figure 4.9. When the pristine QDs were inkjet-printed, they formed droplets with a diameter of $\sim 250 \mu\text{m}$ just after jetting ($t = 0 \text{ s}$) and the size has not changed much until complete drying ($t = 210 \text{ s}$). In the meantime, a hollow center starts to show from $t = 150 \text{ s}$, because most of the QDs have already dried at the edges of the droplet and thus the thickness of the central area decreases rapidly, as confirmed in the height profile in Figure 4.8b. In addition, sharp contour lines inside the droplet are observed in the early phase (from $t = 60 \text{ s}$), which means that the height of the droplet is decreasing over time while the contact line is pinned. Therefore, the final droplet exhibits a shape close to a coffee-ring. It is also supported by the short drying time of $\sim 60 \text{ s}$ for the central area, from $t = 150 \text{ s}$ to 210 s , until complete drying (see Figure 4.9a). On the other hand, the droplet drying process appears differently when a small amount of PMMA is mixed into the QD inks. As shown in Figure 4.9b, from the beginning ($t = 60 \text{ s}$), the droplet of the QD–PMMA composite shrunk smaller and smaller with weak contour lines, resulting in a reduced droplet size. Therefore, it is supposed that the coffee ring effect is effectively suppressed by depinning of contact line by the addition of PMMA. The dynamics of contact line pinning or depinning highly depends on the internal flow dynamics, such as the capillary flow and the Marangoni flow; if the

capillary flow is stronger than the Marangoni flow, contact line pinning can occur easily.[46] As shown above, the viscosity and contact angles of the inks were not significantly changed before and after mixing PMMA. We thus can infer that the Marangoni flow in the droplet is increased when PMMA is mixed into QDs, which is similar to a few previous reports on the Marangoni effect in polymer films.[42,43,47] This is also supported by the extended complete drying time (i.e., ~1320 s) of the composite droplet and its improved uniformity.

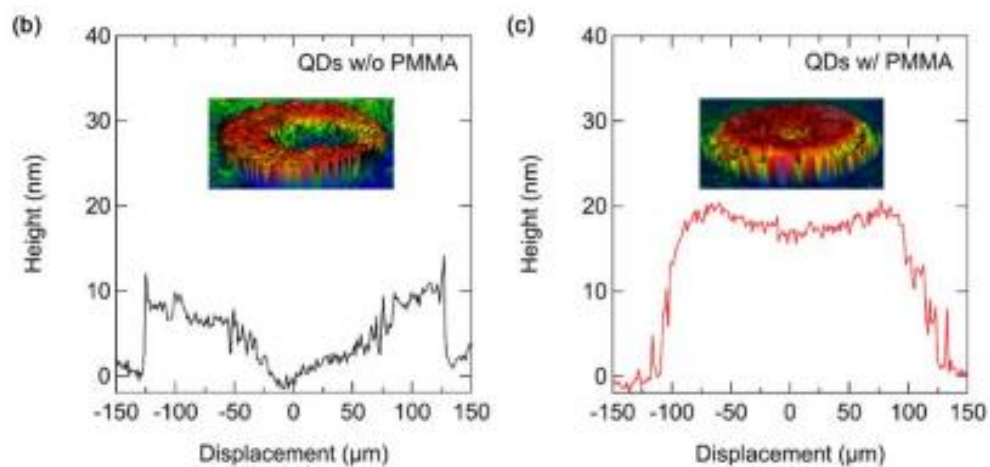


Figure 4.8 The height profile and the 3D morphology images of each droplet from the QD inks (a) without and (b) with PMMA ($M_w = 8$ kDa)

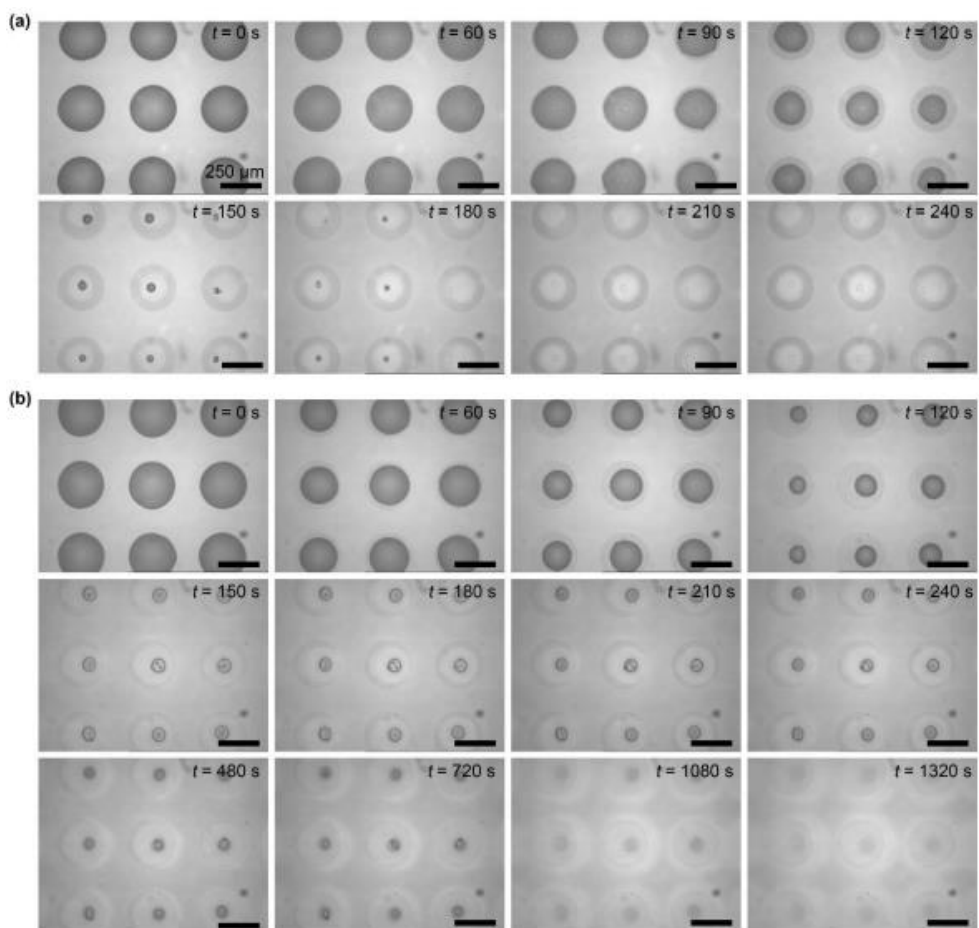


Figure 4.9 Timeline images of drying process for emissive dots using (top) pristine QD ink, (bottom) QD + PMMA ink (Mw : 8 kDa); The time moves from left to right on the timeline.

4.3. Evaluation of QD-PMMA Composite Ink on Pixelated Structure

4.3.1. Morphology Properties of QD Inks on Pixelated Structure

In order to develop practical inkjet-printed QLED displays, QD sub-pixels must be patterned with a pixelated bank structure. However, as opposed to forming a droplet, it is difficult to inkjet-print a thin QD layer uniformly in a pixelated bank. For instance, QDs can pile-up at the edges of the bank toward the bank wall while drying due to the step height and/or surface energy difference between the bank wall and the underlying semiconductor surface. We thus printed the prepared QD inks (with and without PMMA) on a bank structure with a ZnO NP layer at the bottom which is the electron transport layer of the inverted QLEDs. Figure 4.10a shows the microscopic images of the empty sub-pixel array defined by the patterned PI layer and that successfully filled with the inkjet-printed QD-PMMA ink before drying. The dimension of each sub-pixel is $60\ \mu\text{m}$ (width) \times $180\ \mu\text{m}$ (height) with $55\text{-}\mu\text{m}$ spacing.

Figure 4.10b shows the cross-sectional optical profiles of a single sub-pixel consisting of the PI bank, the ZnO NP layer, and the inkjet-printed QD films with various PMMA Mw on the ZnO layer. The thicknesses of the flat and uniform area for both of the pristine QD film and the QD-PMMA films were comparable to $\sim 16\ \text{nm}$. However, a noticeable difference at the edges of

the bank can be found between the pristine QD film and the QD–PMMA composite films: In the pristine QD film, a sizable amount of QDs is piled-up close to the boundaries of the sub-pixel which results in a U-shaped profile, whereas all of the QD–polymer composite films show fine edges without QD accumulation. It may be attributed to the change of internal flow dynamics with slow drying time when PMMA is added into the QD ink, as described above.

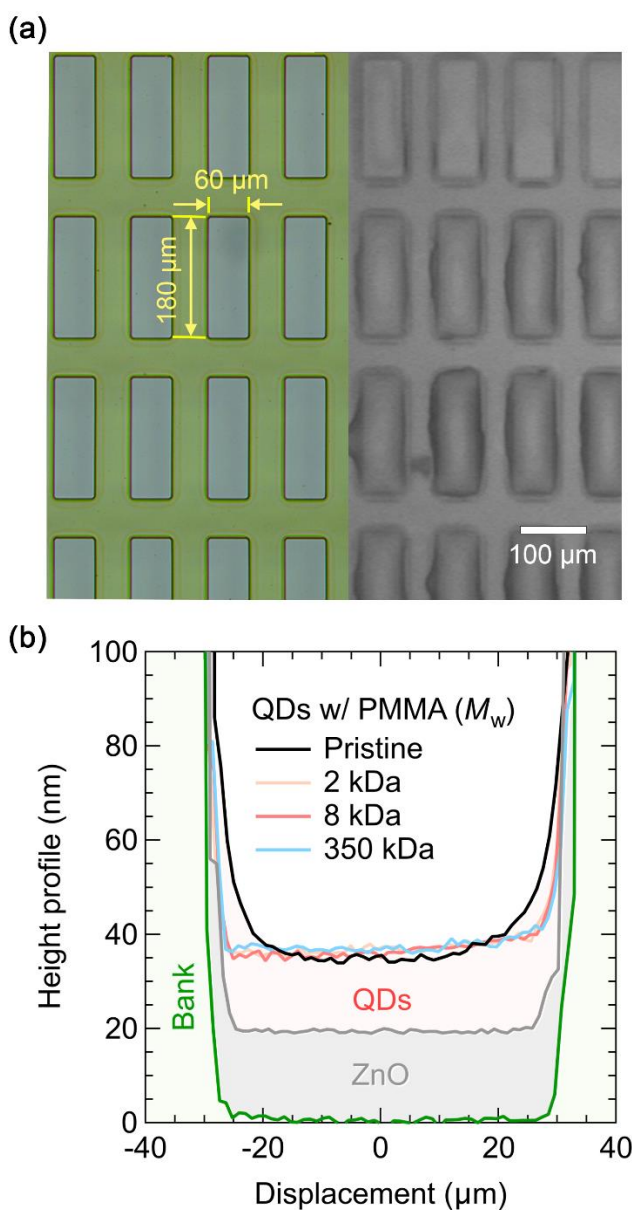


Figure 4.10 (a) Microscope image of subpixel (left) and with inkjet-printed QD films on the bank covered with ZnO NPs (right); yellow line indicates dimensions of sub-pixel; red line indicates cutline for optical profile of horizontal axis, (b) Optical profiles of inkjet-printed films using pristine QD ink and QD + PMMA inks (M_w : 2 kDa, 8 kDa, and 350 kDa, respectively).

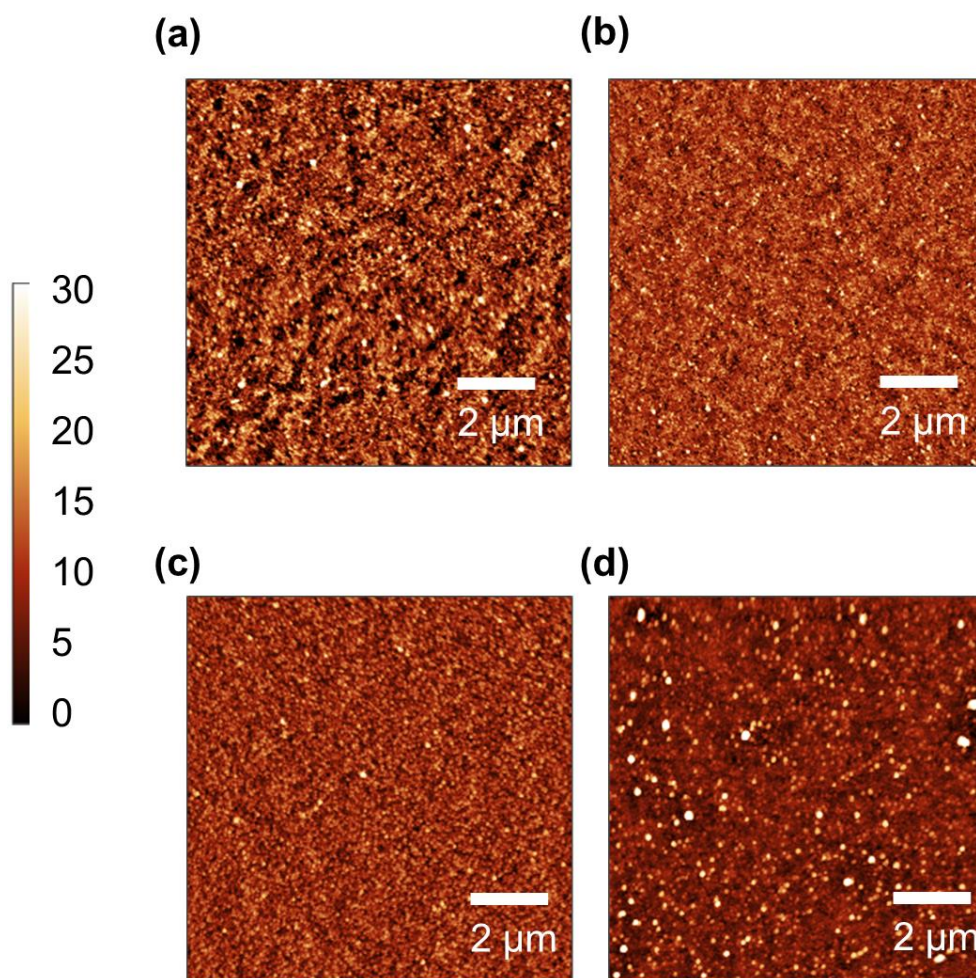


Figure 4.11 AFM images of films using (a) pristine QD ink and QD + PMMA inks (M_w : 2 kDa, 8 kDa, and 350 kDa, respectively), which are inkjet-printed on the bank structure covered with ZnO NPs.

The QD–PMMA composite film also showed improved surface morphology. Figure 4.11 shows the AFM images of the center area of the QD and QD–polymer composite films with different M_w inkjet-printed on a ZnO

layer in the pixelated bank structure. The corresponding root-mean-square (RMS) surface roughness was 5.4 nm (pristine QDs), 3.8 nm, 3.2 nm, and 5.6 nm per order of Mw, respectively. The pristine QD film shows a rough surface (Figure 4.11a), whereas the QD films with PMMA Mw of 2 kDa and 8 kDa show much smoother surfaces. This decreased roughness is attributed to the slow drying process of the QD–polymer composite ink and vacancy filling by PMMA. But when the molecular weight of PMMA was 350 kDa, the surface roughness increased abruptly, resulting from the phase separation and/or self-aggregation of long-chain PMMA.[48]

4.3.2 Electrical Characteristics of Inkjet-printed QLEDs employing PMMA Additives

We fabricated the pixelated, inverted QLEDs with a structure of indium-tin-oxide (ITO)/ZnO NPs (20 nm)/inkjet-printed QD or QD–PMMA composite (16 nm)/4,4'-bis(N-carbazolyl)-1,1'biphenyl (CBP, 60 nm)/MoO₃ (10 nm)/Al (130 nm). The performance of the pixelated QLEDs in terms of the current density (J)–voltage (V), luminance (L)–voltage, the EQE–current density, and the EL spectra, is plotted in Figure 4.12a– 4.12d, respectively. The performance of each device was obtained from 55 sub-pixels of which the total emission area is 0.594 mm². As shown in the J–V curves, the current density of the devices using the pristine QD ink and the QD–polymer composite ink with a PMMA Mw of 2 kDa and 8 kDa does not show a significant difference,

whereas that of the device with 350 kDa PMMA shows decreased J. Additionally, the inset in Figure 4.12a compares the J characteristics at a low voltage region, showing the highest leakage current when the PMMA Mw is 350 kDa. This might originate from the rough morphology in the composite film with PMMA 350 kDa due to phase separation between PMMA and QDs and aggregation of polymer. Meanwhile, the lowest off current was observed when the PMMA Mw is 8 kDa. We can infer that the PMMA Mw of 8 kDa effectively filled the vacancies between the QDs in the composite film, as previously reported in the spin-coated devices.[44] Figure 4.12b shows the L–V characteristics of the devices. When the PMMA Mw of 8 kDa was used, the maximum L of an inkjet-printed QLEDs reached 73360 cd m^{-2} , which is higher by 2.5 times than the QLEDs with the pristine QD ink. Moreover, this result surpasses other reported results on red-emitting inkjet-printed QLEDs, as compared in Table 4.2. The QLED with 350 kDa PMMA exhibits the maximum L of 29718 cd m^{-2} which is similar to that of the pristine QD device. The turn-on voltages (corresponding to the luminance of 1 cd m^{-2}) of the devices with the pristine QD ink and the QD–PMMA (2 kDa and 8 kDa) composite inks were almost the same as 2.3–2.4 V. However, the turn-on voltage of the 350 kDa PMMA device was largely increased to 3.0 V, meaning that long-chain polymers hinder carrier injection into QDs. The effect of PMMA on the EQE is shown in Figure 4.12c. The maximum EQE of the inkjet-printed QLED with the pristine QD ink was 1.0%. When PMMA was added into the ink, the EQEs increased over the entire current density regime. In

particular, the maximum EQE of the device with 8 kDa PMMA was 2.8%, which is 2.8 times higher than the pristine QD device. Even the device with 350 kDa PMMA exhibited higher efficiency than the pristine QD device. It indicates that the QD–PMMA composite is an easy but highly effective method to improve the performance of inkjet-printed QLEDs. As shown in Figure 4.12d, there is no difference in their EL spectra between the devices. For all devices, the peak wavelength and the full-width at half-maximum linewidth were 630 nm and 30 nm, respectively, and the corresponding color coordinates in the Commission Internationale de l'éclairage (CIE) xy chromaticity diagram were (0.69, 0.31). The overall performance of the inkjet-printed, pixelated QLEDs is summarized in Table 4.2.

The photograph in Figure 4.13 shows clear electroluminescence (EL) emission from the inkjet-printed QLED pixel array with the QD–PMMA (8 kDa) composite film. Figure 4.13a and 13b show the microscopic photographs of the sub-pixels of the QLEDs under a bias condition using the pristine QD ink and the QD–PMMA (8 kDa) ink, respectively, which confirms the importance of the QD profile inside the bank. In the images, yellow dashed lines indicate the border of the bank. In the case of the QLED sub-pixels using the pristine QD ink, the region at the edge/corner of the sub-pixel is shaded (Figure 4.13). This is because pile-up of QDs occurs at the edges of the pixelated bank, as explained in the optical profile in Figure 4.10b. Contrary to this, the device with QD–PMMA shows clear edges and homogeneous

emission over the entire area. Therefore, it is thought that using QD–polymer composite inks is highly advantageous for inkjet-printed, pixelated QLEDs.

Figure 4.14 shows lifetime comparison of devices such as pristine QD and QD + PMMA (2 kDa, 8 kDa and 350 kDa of molecular weight). Device lifetime equals device performance trend, but overall lifetime is short.

Figure 4.15 shows the electrical characteristics of EL spectra of the spin-coated QLED and inkjet-printed QLEDs using toluene, mixture and mixture containing polymer additive (Mw: 8 kDa), respectively. The overall performances of the spin-coated and inkjet-printed devices are summarized in Table 4.3. Although the efficiency has been greatly increased by adding polymer to quantum dot ink, it is still short of a well-packaged tendency of QDs by spin coating. However, we believe that further optimization can increase efficiency in inkjet-printed QLEDs.

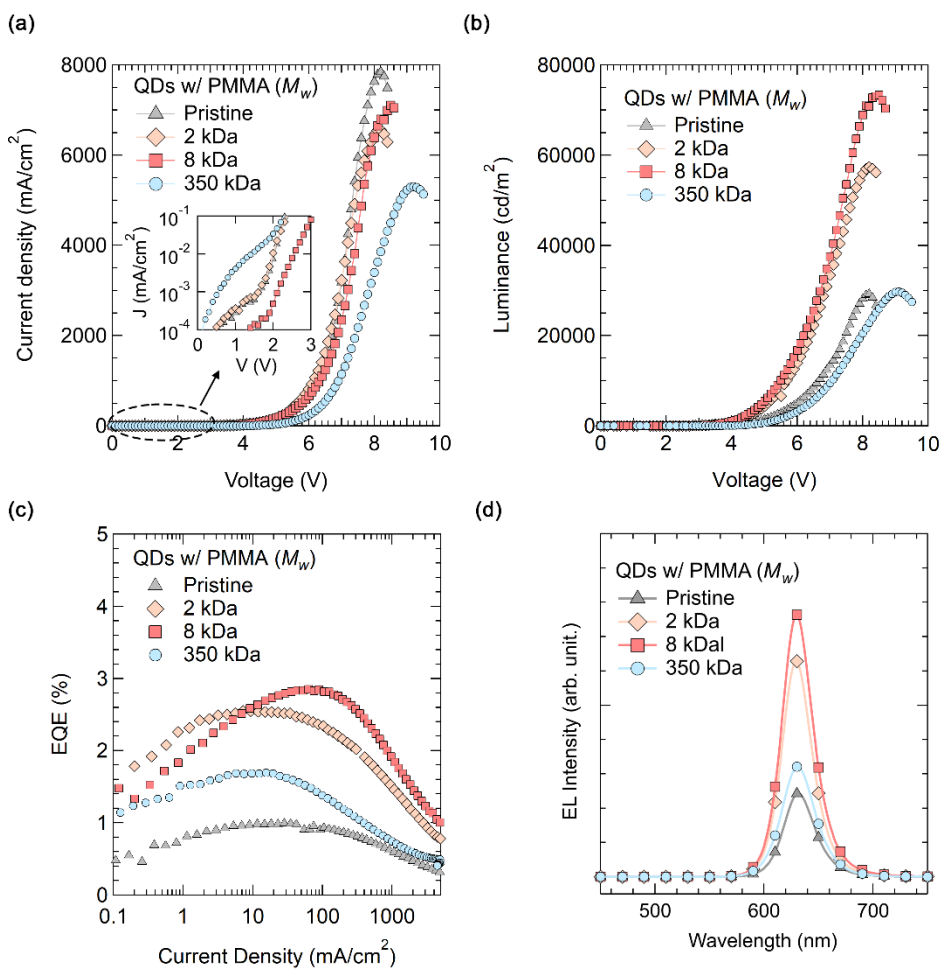


Figure 4.12 (a) Current density–voltage characteristics (inset for a low voltage region), (b) luminance–voltage characteristics, (c) EQE–current density, and (d) the EL spectra of the inkjet-printed QLEDs using the pristine QD ink and the QD–PMMA inks.

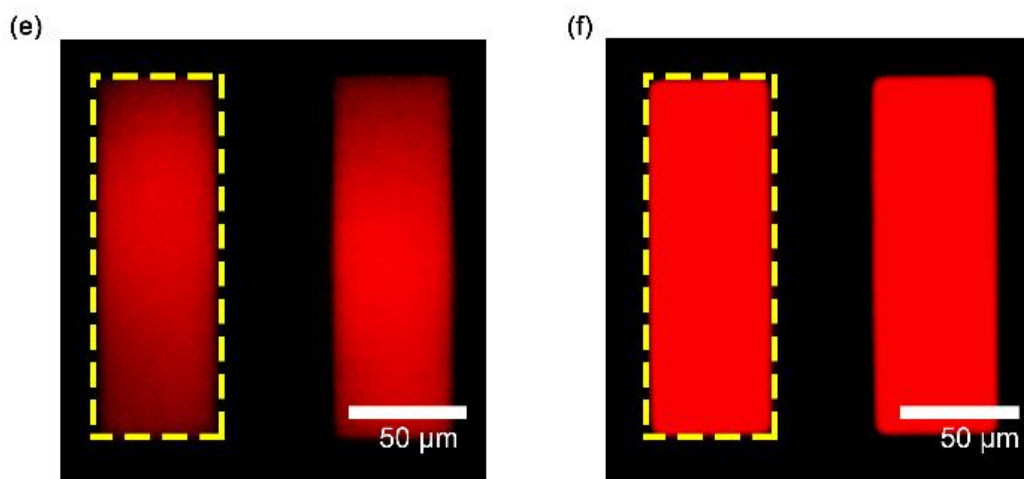


Figure 4.13 Electroluminescence image of (a) pristine QD and (b) QD + PMMA (8 kDa of molecular weight).

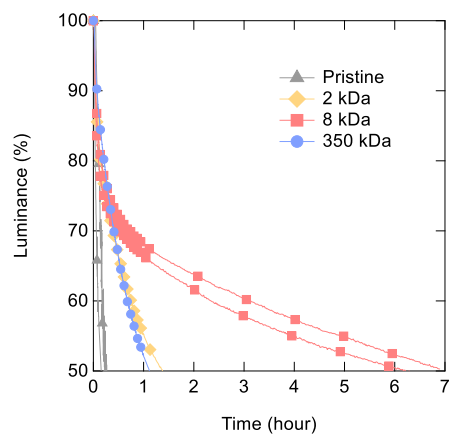


Figure 4.14 Lifetime comparison of pristine QD and QD + PMMA (2 kDa, 8 kDa and 350 kDa of molecular weight). Device lifetime equals device performance trend.

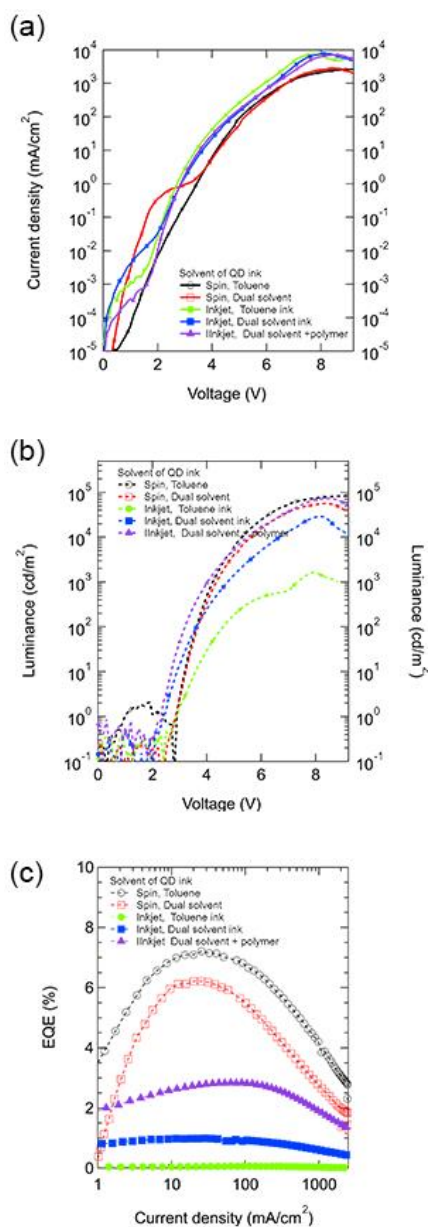


Figure 4.15 (a) Current density–voltage characteristics (inset for a low voltage region), (b) luminance–voltage characteristics, and (c) EQE– current density of the spin-coated QLED and inkjet-printed QLEDs using toluene, mixture and mixture containing polymer additive (Mw: 8 kDa), respectively.

Table 4.2. Parameters for inkjet-printed QLEDs devices using pristine QD ink and QD + PMMA inks (M_w : 2 kDa, 8 kDa, and 350 kDa, respectively):

Mw of PMMA [kDa]	Maximum EQE [%]	Maximum CE [cd A ⁻¹]	Maximum Luminance [cd m ⁻²]	Turn-on Voltage ^{a)} [V]
Pristine	1.0	1.1	29264	2.4
2	2.6	3.0	57368	2.3
8	2.8	3.3	73360	2.3
350	1.7	2.0	29718	3.0

a) The operating voltage corresponding to the luminance of 1 cd m⁻².

Table 4.3. Parameters for spin-coated QLED and inkjet-printed QLEDs devices using toluene, mixture and mixture containing polymer additive (M_w : 8 kDa), respectively.

Solvent	Method	Turn-on Voltage ^{a)} [V]	Max EQE	Max Luminance
Toluene	Spin coating	2.9 V	7.2 %	82617
Dual solvent		2.9 V	5.3 %	56570
Toluene	Inkjet printing	2.9 V	0.1 %	1623
Dual solvent		2.4 V	1.0 %	28264
Dual solvent +polymer		2.3 V	2.9 %	73360

a) The operating voltage corresponding to the luminance of 1 cd m⁻².

4.4 Summary

In summary, we showed that the morphology of inkjet-printed QD films can be improved with the QD–PMMA composite inks by controlling the internal flow dynamics. We also presented that inkjet-printing the composite inks improves the homogeneity of the films inside the bank. The cross-sectional optical profiles and the EL images of a single sub-pixel divine the reduced pile-up at the edges of the bank, showing the importance of the results. As a result, the inkjet-printing based pixelated QLEDs using them exhibited enhanced efficiency and remarkably high luminance without significant detriment to other optical and electrical properties. Therefore, we think that this strategy can be widely applicable for future research on pixelated QLEDs based on inkjet-printing toward large-area full-color QLED displays.

Chapter 5

Conclusion

In this thesis, we devised inkjet-printed QLEDs employing highly fluorinated photopolymer with enhanced printing accuracy and QD-polymer composite ink with enhanced device performance. Using fluorinated photoresist with positive tone, the printing uniformity and the resistance to printing failure promotes. Hydrophobic walls are used making the droplet positing precise within the bank and it is evaluated a photolithographic property and the resistivity on the printing failure of this material. QD-polymer composite ink can increase viscosity of ink and induce the additional polymer Marangoni effect. We showed that the morphology of inkjet-printed QD films can be improved with the QD-PMMA composite inks by controlling the

internal flow dynamics. The inkjet-printing based pixelated QLEDs using QD-PMMA composite ink exhibited enhanced efficiency and remarkably high luminance without significant detriment to other optical and electrical properties.

First, when using hydrophobic walls, printed QD ink with the angular deviation is positioned well in the bank and prevent from the overflow out of emission area. Well defined ink induces the pixel uniformity of devices and resulted QLED exhibit the maximum luminance of 5300 cd m^{-2} and the external quantum efficiency of 0.11 %. Despite of these relatively low performance, it shows the resistivity of printing failure, so I believe it can be further improved through elaborated optimization.

Also, when PMMA is added in the QD ink, the QD-polymer composite ink can reduce the coffee-ring effect and form a uniform thin film. We also presented that inkjet-printing the composite inks improves the homogeneity of the films inside the bank. The cross-sectional optical profiles and the EL images of a single sub-pixel divine the reduced pile-up at the edges of the bank, showing the importance of the results. The resulting inkjet-printed QLED emit the highest luminance of $73,360 \text{ cd m}^{-2}$ and the external quantum efficiency of 2.8 %, which are conspicuously higher than that of the inkjet-printed QLED without polymer additives.

In conclusion, this thesis offers a strategy to enhance printing accuracy and performance of inkjet printed QLEDs. These results lie in a same line with previous studies that reported the impact of charge injection balance on the

device performance, and suggest that the equalized charge injection will enable complete eradication of device degradation factors and promise prolonged operation lifetime of QD-LEDs. Apparent next step to enhance device operational stability is realizing the complete balance in charge injection in QDs by reducing the energy barrier between HTL and the QD emissive layer. We believe that engineering at the interface between QDs and HTL will certainly enable the complete charge injection balance and a long-lived QD-LED.

Bibliography

- [1] A. I. Ekimov, A. L. Efros and A. A. Onushchenko. "Quantum size effect in semiconductor microcrystals." *Solid State Communications*, **56**, 921 (1985).
- [2] R. Rossetti, S. Nakahara and L. E. Brus. "Quantum size effects in the redox potentials, resonance Raman spectra, and electronic spectra of CdS crystallites in aqueous solution." *The Journal of Chemical Physics*, **79**, 1086 (1983).
- [3] A. P. Alivisatos. "Semiconductor Clusters, Nanocrystals, and Quantum Dots." *Science*, **271**, 933 (1996).
- [4] W. K. Bae, S. Brovelli and V. I. Klimov. "Spectroscopic insights into the performance of quantum dot light-emitting diodes." *MRS bulletin*, **38**, 721 (2013).
- [5] V. I. Klimov. *Nanocrystal quantum dots*. 2nd ed., CRC Press: Boca Raton (2010).
- [6] C. B. Murray, C. R. Kagan and M. G. Bawendi. "Synthesis and Characterization of Monodisperse Nanocrystals and Close-Packed Nanocrystal Assemblies." *Annual Review of Materials Science*, **30**, 545 (2000).
- [7] S. Coe, W.-K. Woo, M. Bawendi and V. Bulović. "Electroluminescence from single monolayers of nanocrystals in molecular organic devices." *Nature*, **420**, 800 (2002).
- [8] V. L. Colvin, M. C. Schlamp and A. P. Alivisatos. "Light-emitting diodes made from cadmium selenide nanocrystals and a semiconducting polymer." *Nature*, **370**, 354 (1994).
- [9] T. Kim, K.-H. Kim, S. Kim, S.-M. Choi, H. Jang, H.-K. Seo, H. Lee, D.-Y. Chung and E. Jang. "Efficient and stable blue quantum dot light-emitting diode." *Nature*, **586**, 385 (2020).
- [10] J. Song, O. Wang, H. Shen, Q. Lin, Z. Li, L. Wang, X. Zhang and L. S. Li. "Over 30% External Quantum Efficiency Light-Emitting Diodes by

Engineering Quantum Dot-Assisted Energy Level Match for Hole Transport Layer." *Advanced Functional Materials*, **29**, 1808377 (2019).

[11] B. Dubertret, P. Skourides, D. J. Norris, V. Noireaux, A. H. Brivanlou and A. Libchaber. "In Vivo Imaging of Quantum Dots Encapsulated in Phospholipid Micelles." *Science*, **298**, 1759 (2002).

[12] A. G. Pattantyus-Abraham, I. J. Kramer, A. R. Barkhouse, X. Wang, G. Konstantatos, R. Debnath, L. Levina, I. Raabe, M. K. Nazeeruddin, M. Grätzel and E. H. Sargent. "Depleted-Heterojunction Colloidal Quantum Dot Solar Cells." *ACS Nano*, **4**, 3374 (2010).

[13] I. L. Medintz, H. T. Uyeda, E. R. Goldman and H. Mattoussi. "Quantum dot bioconjugates for imaging, labelling and sensing." *Nature Materials*, **4**, 435 (2005).

[14] D. J. H. A. D. S. C.-S. DR. JONATHAN S. STECKEL, QD VISION. "QDs Generate Light for Next-Generation Displays." (2014).

[15] W. K. Bae, J. Kwak, J. Lim, D. Lee, M. K. Nam, K. Char, C. Lee and S. Lee. "Multicolored Light-Emitting Diodes Based on All-Quantum-Dot Multilayer Films Using Layer-by-Layer Assembly Method." *Nano Letters*, **10**, 2368 (2010).

[16] T. Zhu, K. Shanmugasundaram, S. C. Price, J. Ruzyllo, F. Zhang, J. Xu, S. E. Mohney, Q. Zhang and A. Y. Wang. "Mist fabrication of light emitting diodes with colloidal nanocrystal quantum dots." *Applied Physics Letters*, **92**, 023111 (2008).

[17] H. Cho, J. Kwak, J. Lim, M. Park, D. Lee, W. K. Bae, Y. S. Kim, K. Char, S. Lee and C. Lee. "Soft Contact Transplanted Nanocrystal Quantum Dots for Light-Emitting Diodes: Effect of Surface Energy on Device Performance." *ACS Applied Materials & Interfaces*, **7**, 10828 (2015).

[18] Y. Liu, F. Li, Z. Xu, C. Zheng, T. Guo, X. Xie, L. Qian, D. Fu and X. Yan. "Efficient All-Solution Processed Quantum Dot Light Emitting Diodes Based on Inkjet Printing Technique." *ACS Applied Materials & Interfaces*, **9**, 25506 (2017).

[19] H. M. Haverinen, R. A. Myllylä and G. E. Jabbour. "Inkjet printing of light emitting quantum dots." *Applied Physics Letters*, **94**, 073108 (2009).

[20] W. K. Bae, Y.-S. Park, J. Lim, D. Lee, L. A. Padilha, H. McDaniel, I. Robel, C. Lee, J. M. Pietryga and V. I. Klimov. "Controlling the influence of Auger recombination on the performance of quantum-dot light-emitting diodes." *Nature Communications*, **4**, 2661 (2013).

[21] J. Kwak, W. K. Bae, D. Lee, I. Park, J. Lim, M. Park, H. Cho, H. Woo, D. Y. Yoon, K. Char, S. Lee and C. Lee. "Bright and Efficient Full-Color Colloidal Quantum Dot Light-Emitting Diodes Using an Inverted Device Structure." *Nano Letters*, **12**, 2362 (2012).

[22] J. Son, H. Roh, H. Y. Shin, K.-W. Park, C. Park, H. Park, C. Lee, J. Kwak, B. J. Jung and J.-K. Lee. "Photo-cleavable perfluoroalkylated copolymers for tailoring quantum dot thin films." *Polymer Chemistry*, **11**, 6624 (2020).

- [23] C. Pacholski, A. Kornowski and H. Weller. "Self-assembly of ZnO: From nanodots to nanorods." *Abstracts of Papers of the American Chemical Society*, **224**, U351 (2002).
- [24] D. K. Owens and R. C. Wendt. "Estimation of the surface free energy of polymers." *Journal of Applied Polymer Science*, **13**, 1741 (1969).
- [25] H. Hu and R. G. Larson. "Marangoni Effect Reverses Coffee-Ring Depositions." *The Journal of Physical Chemistry B*, **110**, 7090 (2006).
- [26] T. Kajiyama, W. Kobayashi, T. Okuzono and M. Doi. "Controlling the Drying and Film Formation Processes of Polymer Solution Droplets with Addition of Small Amount of Surfactants." *The Journal of Physical Chemistry B*, **113**, 15460 (2009).
- [27] T. Kajiyama, C. Monteux, T. Narita, F. Lequeux and M. Doi. "Contact-Line Recession Leaving a Macroscopic Polymer Film in the Drying Droplets of Water–Poly(N,N-dimethylacrylamide) (PDMA) Solution." *Langmuir*, **25**, 6934 (2009).
- [28] N. Lin, Y. Ye, Q. Guo, J. Yu and T. Guo. "Effect of using ink containing polyacrylate and silicone surfactant on the inkjet printing of quantum dot films." *Journal of Information Display*, **21**, 113 (2020).
- [29] D. M. Paeasch, A.; "Marangoni effects in the spreading of liquid mixtures on a solid." *Langmuir*, **3**, 519 (1987).
- [30] D. Pesach and A. Marmur. "Marangoni effects in the spreading of liquid mixtures on a solid." *Langmuir*, **3**, 519 (1987).
- [31] C. Poulard and P. Damman. "Control of spreading and drying of a polymer solution from Marangoni flows." *Europhysics Letters (EPL)*, **80**, 64001 (2007).
- [32] W. D. Ristenpart, P. G. Kim, C. Domingues, J. Wan and H. A. Stone. "Influence of Substrate Conductivity on Circulation Reversal in Evaporating Drops." *Physical Review Letters*, **99**, 234502 (2007).
- [33] T. Still, P. J. Yunker and A. G. Yodanis. "Surfactant-Induced Marangoni Eddies Alter the Coffee-Rings of Evaporating Colloidal Drops." *Langmuir*, **28**, 4984 (2012).
- [34] R. Xing, T. Ye, Y. Ding, Z. Ding, D. Ma and Y. Han. "Thickness Uniformity Adjustment of Inkjet Printed Light-emitting Polymer Films by Solvent Mixture." *Chinese Journal of Chemistry*, **31**, 1449 (2013).
- [35] X. Xu and J. Luo. "Marangoni flow in an evaporating water droplet." *Applied Physics Letters*, **91**, 124102 (2007).
- [36] C. Jiang, Z. Zhong, B. Liu, Z. He, J. Zou, L. Wang, J. Wang, J. Peng and Y. Cao. "Coffee-Ring-Free Quantum Dot Thin Film Using Inkjet Printing from a Mixed-Solvent System on Modified ZnO Transport Layer for Light-Emitting Devices." *ACS Applied Materials & Interfaces*, **8**, 26162 (2016).
- [37] B. Geffroy, P. le Roy and C. Prat. "Organic light-emitting diode (OLED) technology: materials, devices and display technologies." *Polymer International*, **55**, 572 (2006).

- [38] V. V. Khatavkar, P. D. Anderson, P. C. Duineveld and H. H. E. Meijer. "Diffuse Interface Modeling of Droplet Impact on a Pre-Patterned Solid Surface." *Macromolecular Rapid Communications*, **26**, 298 (2005).
- [39] T. Liou, C. Chan, C. Fu and K. Shih. "Effects of Impact Inertia and Surface Characteristics on Deposited Polymer Droplets in Microcavities." *Journal of Microelectromechanical Systems*, **17**, 278 (2008).
- [40] D. Y. Kim, Y. J. Han, J. Choi, C. Sakong, B.-K. Ju and K. H. Cho. "Inkjet printed quantum dot film formed by controlling surface wettability for blue-to-green color conversion." *Organic Electronics*, **84**, 105814 (2020).
- [41] N. Felix and C. K. Ober. "Acid-Labile, Chain-Scission Polymer Systems Used as Positive-Tone Photoresists Developable in Supercritical CO₂." *Chemistry of Materials*, **20**, 2932 (2008).
- [42] E. Reichmanis and G. Smolinsky. "Oxygen RIE-Resistant Deep-UV Positive Resists: Poly (trimethylsilylmethyl methacrylate) and Poly (trimethylsilylmethyl methacrylate-co-3-oximo-2-butanone methacrylate)." *Journal of The Electrochemical Society*, **132**, 1178 (1985).
- [43] R. D. Deegan. "Pattern formation in drying drops." *Physical Review E*, **61**, 475 (2000).
- [44] R. D. Deegan, O. Bakajin, T. F. Dupont, G. Huber, S. R. Nageland T. A. Witten. "Capillary flow as the cause of ring stains from dried liquid drops." *Nature*, **389**, 827 (1997).
- [45] R. D. Deegan, O. Bakajin, T. F. Dupont, G. Huber, S. R. Nageland T. A. Witten. "Contact line deposits in an evaporating drop." *Physical Review E*, **62**, 756 (2000).
- [46] J. Wang, T. Dong, Z. Zhong, H. Zheng, W. Xu, L. Ying, J. Wang, J. Peng and Y. Cao. "Uniform inkjet-printed films with single solvent." *Thin Solid Films*, **667**, 21 (2018).
- [47] X. Yu, R. Xing, Z. Peng, Y. Lin, Z. Du, J. Ding, L. Wang and Y. Han. "To inhibit coffee ring effect in inkjet printing of light-emitting polymer films by decreasing capillary force." *Chinese Chemical Letters*, **30**, 135 (2019).
- [48] B.-J. de Gans and U. S. Schubert. "Inkjet Printing of Well-Defined Polymer Dots and Arrays." *Langmuir*, **20**, 7789 (2004).
- [49] D. Kim, S. Jeong, B. K. Park and J. Moon. "Direct writing of silver conductive patterns: Improvement of film morphology and conductance by controlling solvent compositions." *Applied Physics Letters*, **89**, 264101 (2006).
- [50] P. Tang, L. Xie, X. Xiong, C. Wei, W. Zhao, M. Chen, J. Zhuang, W. Su and Z. Cui. "Realizing 22.3% EQE and 7-Fold Lifetime Enhancement in QLEDs via Blending Polymer TFB and Cross-Linkable Small Molecules for a Solvent-Resistant Hole Transport Layer." *ACS Applied Materials & Interfaces* (2020).
- [51] L. Xie, X. Xiong, Q. Chang, X. Chen, C. Wei, X. Li, M. Zhang, W. Su and Z. Cui. "Inkjet-Printed High-Efficiency Multilayer QLEDs Based

on a Novel Crosslinkable Small-Molecule Hole Transport Material." *Small*, **15**, 1900111 (2019).

[52] Z. Xing, J. Zhuang, C. Wei, D. Zhang, Z. Xie, X. Xu, S. Ji, J. Tang, W. Suand Z. Cui. "Inkjet-Printed Quantum Dot Light-Emitting Diodes with an Air-Stable Hole Transport Material." *ACS Applied Materials & Interfaces*, **9**, 16351 (2017).

[53] X. Xiong, C. Wei, L. Xie, M. Chen, P. Tang, W. Shen, Z. Deng, X. Li, Y. Duan, W. Su, H. Zengand Z. Cui. "Realizing 17.0% external quantum efficiency in red quantum dot light-emitting diodes by pursuing the ideal inkjet-printed film and interface." *Organic Electronics*, **73**, 247 (2019).

[54] R. M. Abozaid, Z. Ž. Lazarević, I. Radović, M. Gilić, D. Šević, M. S. Rabasovićand V. Radojević. "Optical properties and fluorescence of quantum dots CdSe/ZnS-PMMA composite films with interface modifications." *Optical Materials*, **92**, 405 (2019).

[55] A. Badawi. "Characterization of the optical and mechanical properties of CdSe QDs/PMMA nanocomposite films." *Journal of Materials Science: Materials in Electronics*, **26**, 3450 (2015).

[56] Z. Wang, X. Xiao, J. Shen, P. Liu, D. Wu, X. Tang, G. Mei, J. Sun, H. Yang, X. Li, Z. Wu, Q. Xie, F. Fang, S. Ding, W. C. H. Choy, X. W. Sunand K. Wang. "Enhancing stability of CsPbBr₃ nanocrystals light-emitting diodes through polymethylmethacrylate physical adsorption." *Nano Select*, **1**, 372 (2020).

[57] L. Xue, Y. Liu, F. Li, K. Sun, W. Chen, K. Yang, H. Hu, J. Lin, H. Chen, Z. Yangand T. Guo. "Highly flexible light emitting diodes based on a quantum dots-polymer composite emitting layer." *Vacuum*, **163**, 282 (2019).

[58] B. Derby. "Inkjet Printing of Functional and Structural Materials: Fluid Property Requirements, Feature Stability, and Resolution." *Annual Review of Materials Research*, **40**, 395 (2010).

한글 초록

콜로이드성 양자점은 광소자에 사용하기에 적합한 광학적 전기적 특성을 가지고 있다. 특히나 높은 양자효율, 좁은 발광 파장대, 무기 재료의 내적 열안정성과 광안정성을 가지고 있기에 발광다이오드의 광물질로 사용하기에 적합하다. 그러나 양자점 소재는 콜로이드로 용액 공정 기반이기 때문에 차세대 디스플레이로 사용되기 위해서는 패터닝 기술이 매우 중요하다. 드랍 캐스팅 방법, 미스트 코팅 방법, 트랜스퍼 프린팅 등의 다양한 기술들이 보고되어 왔으나 최근에는 물질 소모 최소화와 고해상도 공정이 가능한 잉크젯 기술이 관심받고 있다. 그러나 잉크젯 기술에는 몇 가지 기술적인 이슈로 인해서 잉크젯 프린팅된 양자점 자발광 소자의 성능은 아직까지 스펀코팅 소자에 비해 낮게 보고되고 있다. 최근에는 잉크젯 프린팅 기반의 양자점 자발광 소자는 용매 혼합물과 बैं크 구조물의 표면 에너지를 바꾸는 방식 등으로 많은 연구가 보고되고 있지만 아직 그에 따른 성능을 분석하는 연구는 부족한 상황이다.

잉크젯 프린팅 기술을 이용한 고성능 양자점 발광 다이오드의 제작을 위해서는 몇 가지 도전과제가 있다. 첫 번째는 커피링 효과와 낮은 러프리스를 낮추는 균일한 박막형성이다. 두 번째는 노즐 클로킹, 머신 흔들림, 오류발생 등에 의한 노즐에서 사출된 방울의 각도변화로 인한 프린팅 실패이다. 이로써 미스-에이밍과 오버플로우가 발생한다. 세 번째는 노즐에서 안정된 드랍을 형성하기 위한 제터빌리티이다. 이는 점도, 표면장력, 내부 장력에 의해서 결정지어진다. 마지막은 용매 제한인데, 아래 층을 녹이지 않으면서 양자점

영킹을 막으며 사람에게 유해하지 않을 조건을 가지고 있어야 한다. 잉크젯 양자점 발광 다이오드의 성능을 향상시키기 위해 용매 혼합물을 통해서 균일한 양자점 필름을 만들거나 표면 에너지를 바꾸면서 프린팅 실패를 방지하기 위해서 여러가지 연구들이 있었다. 잉크젯 양자점 발광 다이오드의 실용적인 사용을 위해서, 커피링 효과와 프린팅 실패를 잉크젯 소자의 성능과 관련하여 해결할 필요가 있다.

본 연구에서는 소수성의 폴리머를 픽셀 구조물인 बैं크로 사용해서 프린팅 실패를 보상해 픽셀 균일성을 확보하고, 투명한 폴리머인 PMMA 가 큐디 잉크에 섞였을 때 필름 모포로지 변화와 그 전기적 상황에 대한 연구를 진행하였다.

소수성 격벽을 사용했을 때, 각도 변화가 있는 프린팅된 양자점 잉크가 बैं크 내부에 잘 위치하였고 발광 영역에 벗어나는 오버플로우가 방지하였다. 잘 형성된 잉크는 소자의 픽셀 균일성을 향상시켰고, 결과적인 소자의 성능은 5300 cd m^{-2} 의 밝기와 0.11 % 의 양자 효율을 낼 수 있었다. 비교적 낮은 성능에도 불구하고, 이는 프린팅 실패의 저항성을 보여주었고, 정교한 최적화를 통하면 소자 성능이 보다 나은 향상을 보일 것이라 생각한다.

또한, 양자점 잉크에 PMMA 를 첨가했을 때, 양자점-폴리머 혼합 잉크는 커피링 효과를 줄일 수 있었고 균일한 박막을 형성하였다. बैं크 격벽의 쌓임 현상 또한 추가적인 폴리머 마랑고니 효과를 통하여 줄일 수 있었다. 게다가, 적절한 폴리머 체인 길이의 PMMA 는 표면 거칠기를 줄여서, 소자의 성능도 향상시킬 수 있었다. 결과적인 잉크젯 양자점 발광다이오드는 73360 cd m^{-2} 의 밝기와 2.8 % 의 양자효율로, 폴리머 첨가물을 넣지 않은 잉크젯 양자점 소자의 비해 눈에 띄게 향상되었다.

본 논문에서 개발된 양자점 발광 다이오드의 소자 격벽 구조와 양자점 폴리머 혼합 잉크에 대한 결과는 고효율 잉크젯 양자점 발광다이오드의 실현에 큰 도움이 될 것으로 생각된다.

주요어: 양자점 발광다이오드, 잉크젯 프린팅, 소수성 폴리머, बैंक 엔지니어링, 폴리머 첨가물, 커피링 효과

학번: 2014-22556

감사의 글

어떻게 시간일 흘러 갔는지 모를 정도로 시간이 빨리 지나가서 제가 지금 석·박사 통합 과정을 마치고 박사 졸업을 앞두고 있다는 것이 실감나지 않습니다. 부족했던 제가 이곳까지 올 수 있었던 것은 저 혼자만의 힘이 아닌 지도교수님들, 연구실 선/후배 및 동료분들, 그리고 가족들이 있었기에 가능했다고 생각합니다. 지금까지 모자란 저를 지켜봐 주시고 도와주신 분들께 이 자리를 빌어 감사의 인사를 드리고자 합니다.

먼저 저를 받아주시고 아낌없이 지도해주신 이창희 교수님께 감사드립니다. 교수님께서 지도해주신 연구자로서의 자세를 언제나 마음속에 새기며 교수님께 부끄럽지 않은 제자가 될 수 있도록 노력하겠습니다. 혼란했던 시기에 저희 연구실의 지도교수로 와 주셔서 방향하던 저를 이끌어 주신 곽정훈 교수님께도 감사의 말씀을 드립니다. 교수님의 아낌없는 조언과 가르침 덕분에 제가 연구를 계속할 수 있는 용기를 얻었고 많은 것을 배우고 성장할 수 있었습니다. 앞으로도 교수님께 부끄럽지 않은 제자가 되기 위해 항상 정진하겠습니다. 또한 제 박사학위논문이 다듬어질 수 있도록 지도해주신 홍용택 교수님, 이재상 교수님, 송형준 교수님, 정승준 박사님께도 감사의 인사를 올립니다. 가르침을 잊지 않고, 저도 훌륭한 교수님들처럼 다른 사람들에게 도움이 되는 사람이 되도록 노력하겠습니다.

연구실 생활을 하면서 진로를 포함한 다양한 고민과 걱정들이 하는 일이 많이 있었습니다. 그 때마다, 곁에서 같은 길을 걷어가는 연구실 선/후배, 동료분들이 있었기에 의지하여 힘을 낼 수 있었습니다. 유기 트랜지스터를 연구하던 시절 어리숙했던 저에게 많은 조언을 주시고 도움을 주신 노정균 교수는 저에게 큰 힘이 되었고 연구에 본보기가 되어 주었습니다. 논문 지도와 저에 대해 아낌없는 조언을 해주신 김준영 교수님께도 진심으로 감사드립니다. 트랜지스터를 할 때 부족한 저에게 논문지도 해주시고 여러 경험을 하게 도와주신 김혁 교수님, 정말

감사드립니다. 같이 트랜지스터 하면서 옆에서 고민과 걱정을 나누고 아낌없는 덕담을 해준 현우, 덕분에 많은 힘을 받았습니다. 같은 잉크젯 팀이었지만 양자점 소자를 모르던 저에게 많은 도움을 준 축구대장 종석이, 지금은 다른 연구실이지만 잉크젯 하느라 같이 고생한 동현이, 회계 업무도 관여하고 여러 분야를 하느라 고생하는 천사 예슬이, 바쁘다고 많이 못 챙겨줘서 미안한 똑똑이 민형, 묵묵히 도와줘서 고마웠던 지원이 정말 고마웠습니다. 신입생 때 잘 적응할 수 있도록 도와준 명진이형, 옆에서 덕담을 많이 해준 착한 희영, 자기관리에 철저했던 지호, 호정, 지연, 용원, 연경, 마음 따뜻한 서현, 연구에 열정적인 건식, 멋쟁이 현호 교수, 본보기가 되는 엘리트 재훈이, 옆에서 많이 도와줬던 승현이, 도움주셔서 정말 감사합니다. 같이 졸업 준비하며 고생한 보드게임마스터 영준이, 늘 잘할 거라고 생각되는 부지런한 태수, 볼 때마다 항상 웃던 분위기메이커 경환이, 포토샵 도와줘서 고마웠던 에이스 주형이와 발표 잘하는 수현이, 옆자리에서 응원해준 착한 아영이가 있어 연구실 생활을 무사히 마칠 수 있었습니다. 갑자기 양자점 한다고 고생한 스타대장 재열이, 분야 가리지 않고 열정을 보이며 또 잘하는 올마스터 근우, 공정에 대해 많이 도와준 선홍, 얼마 남지 않은 연구실 생활 모두 무사히 잘 마치길 바랍니다. 앞으로 연구실의 주축이 될 지현이, 연준이, 한솔이도 다들 연구실 생활 잘 해 나가리라 믿고 고마웠어. 귀중한 실험 재료를 제공해주고 함께 연구를 진행했던 배완기 교수님, 준혁 박사, 동효 박사, 이진균 교수님, 손종찬 박사 모두 감사합니다.

사랑하는 아버지, 어머니, 지금까지 보내주신 믿음과 응원에 앞으로도 늘 보답할 수 있는 아들이 될 수 있도록 노력하겠습니다. 하나뿐인 나의 누나, 항상 응원해주시는 할머니를 비롯한 가족분들께도 감사드립니다.

다시 한번 도움을 주신 모든 분들께 감사드리며, 졸업 후에도 언제나 더 발전된 사람이 될 수 있도록 노력하겠습니다.

2021년 2월

노희범